JOURNAL OF GEOPHYSICAL RESEARCH, VOL. 105, NO. D6, PAGES 7111–7131, MARCH 27, 2000

Chlorine activation during the early 1995-1996 Arctic winter

Steven T. Massie, XueXi Tie, and Guy P. Brasseur
National Center for Atmospheric Research, Boulder, Colorado

Richard M. Bevilacqua and Michael D. Fromm
Naval Research Laboratory, Washington, D. C.

Michelle L. Santee
Jet Propulsion Laboratory, California Institute of Technology, Pasadena

Abstract. The coupling of temperature, aerosol area density, and chlorine activation is studied by comparing values from a three-dimensional chemical transport model with observed temperature, aerosol area density, and ClO data in the Arctic for the time period December 1, 1995, to January 9, 1996. The three-dimensional model uses United Kingdom Meteorological Office (UKMO) winds and temperatures, run on pressure surfaces between 316 and 0.31 hPa, and the model results are examined at 100, 68, 46, 31, and 21 hPa. Radiosonde values are compared to individual UKMO temperature values to assess the impact of model temperature errors upon heterogeneous chemistry reaction probabilities. Polar Ozone and Aerosol Measurement (POAM II) aerosol extinction values are transformed into area density values and compared to model daily averaged time trends. The model is run with gas phase chemistry only, gas phase plus sulfate aerosol chemistry, and the case where gas phase, sulfate aerosol, and polar stratospheric cloud reactions are active. Results from these calculations are used to examine the sensitivity of chlorine activation to temperature biases, area density uncertainties, and the effects of the reaction paths OH + ClO -> HCl + O_2 (4% yield) and HO_2 + ClO -> HCl + O_3 (4% yield). Sulfate aerosol is demonstrated to be very effective in activating chlorine in the Arctic polar vortex. Time trends of five-day averages of model and Upper Atmosphere Research Satellite (UARS) Microwave Limb Sounder (MLS) version 4 ClO over extended regions inside and outside the vortex at 21 and 46 hPa agree within the experimental error.

1. Introduction

The conceptual framework of chlorine activation and subsequent loss of ozone in the polar regions is well established [*World Meteorological Organization (WMO)*, 1995]. Heterogeneous reactions on cold aerosol particles convert inactive chlorine molecules ($ClONO_2$, HCl) into Cl_2 and HOCl, which are then photolyzed into chlorine atoms. Cl and ClO are in photochemical equilibrium during the day, while ClO is transformed during the night into the chlorine dimer (Cl_2O_2). Photolysis of the dimer regenerates active chlorine. Cl decreases the O_3 concentration in the polar regions by ~ 1% per day when active chlorine is present [*Salawitch et al.*, 1993]. Changes in the ozone abundance are mainly due to chemical loss and to transport from above. The chemistry takes place in polar vortices that are dynamically isolated in the winter from other stratospheric regions.

There are several studies, however, which report that model calculations underestimate the amount of ozone loss which is observed near the 460 K potential temperature surface in both the southern and northern polar regions. (See Table 1 for the correspondence between pressure and potential temperature for vortex averaged temperature values.) *Chipperfield et al.* [1996] compare SLIMCAT three-dimensional chemical transport calculations of ozone loss with Upper Atmosphere Research Satellite (UARS) Antarctic data for September 1992. *Chipperfield et al.* [1996, Figures 3 and 7] showed that ClO and ozone loss are both underestimated in the inner vortex at 465 K, though at 585 K, ozone loss is overestimated. *Deniel et al.* [1998] compare REPROBUS (reactive processes ruling the ozone budget in the stratosphere) three-dimensional chemistry transport calculations of ozone loss with that observed by the Polar Ozone and Aerosol Measurement (POAM II) solar occultation instrument during the 1994-1995 Arctic winter. Observed ozone loss on the 400 and 650 K potential temperature surfaces agrees well with model values. However, at both 430 and 470 K, the calculated ozone loss is underestimated by 30%. These studies illustrate that there are unresolved quantitative differences between observation and three-dimensional models.

Validation of the qualitative framework requires quantitative comparisons of observation and model results at each cause and effect link: (1) temperature, (2) generation of aerosol area density, (3) conversion of inactive chlorine to active chlorine on aerosol surfaces, and (4) ozone loss. Our initial intention was to study the full time period from December 1, 1995, through March 31, 1996, examine links (1) through (4) in a thorough analysis, and to compare observed and model ozone loss inside and outside of the vortex. However, calculations by W. Randel and F. Wu (personal communication, 1998) demonstrated that

Paper number 1999JD901035.
0148-0227/00/1999JD901035$09.00

our model vertical motion field, based on the analyses produced by the United Kingdom Meteorological Office (UKMO) stratospheric assimilation, displayed $\overline{w}^*$ (transformed Eulerian zonal mean) values which had a net upward component, in stark contrast to an expected downward component of flow into the vortex. We have therefore limited our study to a shorter time period, from December 1, 1995, through January 9, 1996, to minimize the effect of long-term vertical transport and to analyze only links (1) through (3).

The focus of this paper is to examine the coupling between temperature, aerosol area density, and the activation of chlorine in the early Arctic winter. Model values of temperature, area density, and ClO mixing ratios are compared to observations. Calculations are carried out to examine the sensitivity of chlorine activation upon uncertainties in temperature values, upon particle composition type, upon the magnitude of the aerosol area density, and upon differences in new and older heterogeneous rates of reaction.

Our study is presented in the following manner. Section 2 discusses the observations which are compared to the model values. The three-dimensional chemical transport model is discussed in section 3. Vortex morphology is examined in section 4. Radiosonde temperatures are compared to UKMO temperatures in section 5 in order to assess the sensitivity of heterogeneous reaction probabilities to model temperature errors. POAM II extinction data are transformed into area density values and compared to daily averaged model area density values in section 6. Model and Halogen Occultation Experiment (HALOE) observations of HCl are examined in section 7. MLS ClO mixing ratios are compared to model values in section 8. The influence of $\overline{w}^*$ upon the model calculations is also discussed in section 8. Section 9 summarizes the previous sections and comments upon whether or not the model can reproduce the observed magnitude and rate of chlorine activation.

2. Observations

2.1. Temperature

The three-dimensional chemical-transport model (discussed in section 3) is driven by UKMO wind and temperature fields [*Swinbank and O'Neill*, 1994]. Since gas phase and heterogeneous chemistry are temperature dependent, the model (UKMO) temperature values are compared to radiosonde data in order to assess the influence of model temperature errors upon heterogeneous reaction probabilities. For this study we use the radiosonde data which resides on the UARS Central Data Handling Facility (CDHF). Statistical analysis is performed using daily colocated UKMO and radiosonde temperatures to determine temperature differences between the model and radiosonde values.

The analysis of temperature differences is relevant because earlier studies have noted that temperature uncertainties of several degrees have important impacts upon the interpretation of model and observation comparisons in the polar regions. *Schoeberl et al.* [1993] and *Douglass et al.* [1993] obtained better agreement between model and UARS ClO data comparisons when temperatures were decreased by 2 K.

2.2. Aerosol Extinction

POAM II aerosol extinction data are transformed into area density values in order to compare time trends of observed and model area density values. POAM II is a solar occultation experiment which measures mixing ratios of O_3 and NO_2 in addition to aerosol extinction at 0.352, 0.442, 0.600, 0.781, 0.921, and 1.06 μm with 1 km vertical resolution. The 1.06 μm channel is the primary aerosol channel. The POAM II instrument is discussed by *Glaccum et al.* [1996], and *Lumpe et al.* [1997] discuss the version 5 POAM II retrieval algorithm. Orbital geometry of the SPOT 3 satellite, which carried POAM II, gave rise to occultations between 63° and 65° latitude during the 1995-1996 northern winter.

Randall et al. [1996] present an overview of POAM II aerosol measurements at 1.06 μm and demonstrate that POAM II data between 15 and 24 km agree well with coincident Stratospheric Aerosol and Gas Experiment (SAGE) II extinction values at 1.02 μm. POAM II version 5 data at 1.06 μm is used in this study. Random measurement errors of the version 5 1.06 μm extinction are between 10 and 20% between 15 and 25 km altitude, and the systematic errors are in the 10-15% range [*Lumpe et al.*, 1997].

POAM II extinction data at 1.06 μm were transformed using equation (5) of *Massie et al.* [1998] and the "average" transformation coefficients of *Massie et al.* [1998, Tables 4-6]. These coefficients are based on least squares fits to theoretical extinction values calculated using the Polar Stratospheric Cloud (PSC) and sulfate aerosol size distributions measured by the forward-scattering spectrometer probe (FSSP 300) during the Airborne Arctic Stratospheric Experiment. The least squares fit (for the transformation from theoretical extinction to observed area density) matches the FSSP-300 area density data at 1 μm to within 20%. This transformation yields area densities within 19% rms of those calculated with the middle-latitude sulfate aerosol transformation of *Thomason et al.* [1997] for 1 μm extinction values between 1 x 10^{-5} and 2 x 10^{-3} km^{-1} (i.e., area densities between 0.2 and 5 $micron^2$ cm^{-3}). The transformation error is assigned to be 25%.

Error bars for the area densities are assigned based upon the following considerations. A systematic error of 30% is calculated from the square root sum of the version 5 systematic error of 15% and a transformation error of 25%. The random error is 15% based upon *Lumpe et al.* [1997]. Model calculations are also carried out with sulfate aerosol area densities which are 30% lower than the standard case (discussed below in section 3) in order to examine the sensitivity of chlorine activation to values of initial sulfate area density and to acknowledge the imprecise nature of the transformation between extinction and area density.

2.3. HNO_3

Model calculations are initialized with version 4 Microwave Limb Sounder (MLS) HNO_3 data. A 6-year climatology of this data set is presented by *Santee et al.* [1999] and has been applied in PSC microphysical studies for Antarctic conditions [*Santee et al.*, 1998] and for Arctic conditions [*Massie et al.*, 1997].

Validation studies illustrate that the version 4 MLS HNO_3 mixing ratios are useful on the 100, 46, and 21 hPa retrieval surfaces, with single profile precisions of 2.0, 3.0, and 4.5 ppbv [*Santee et al.*, 1998, W. Froidevaux et al., UARS MLS Data Quality Document, Version 4 Data, available at http://mls.jpl.nasa.gov.]. The MLS HNO_3 data agree well with UARS Cryogenic Limb Array Etalon Spectrometer (CLAES) HNO_3 values at 100 hPa but are usually 0-2 ppbv lower at 46 hPa and 0-4 ppbv higher at 21 hPa [*Santee et al.*, 1998]. The timing and overall morphology of the buildup of HNO_3 in the northern polar vortex are in excellent agreement in the CLAES and MLS data sets [*Santee et al.*, 1999].

2.4. HCl

Ideally, one would like to directly observe the depletion in the polar vortex of HCl, $ClONO_2$, and N_2O_5 as they are converted into reactive chlorine and HNO_3 and to intercompare model and observed N_2O and CH_4 as a check on the model wind field. As noted by *Geller et al.* [1995], it is difficult to find days in which both MLS and HALOE are looking at the same time into the winter hemisphere at latitudes where polar processing is occurring. CLAES observations ceased in May of 1993 when the instrument cryogen was depleted and the HALOE viewing geometry was such that it only began to observe HCl northward of 30° after December 14, 1995. The northernmost latitude observed by HALOE in the December 1, 1995, and January 9, 1996, time period is 48°. Therefore a direct comparison of observed and modeled HCl values throughout and adjacent to the polar vortex during this time period is not possible. Comparisons of HALOE HCl with model values for the latitude range from 30° to 50°N are presented in section 7.

The HALOE instrument is described by *Russell et al.* [1993]. Validation studies of HALOE HCl and CH_4 mixing ratios are presented by *Russell et al.* [1996] and *Park et al.* [1996]. The mean difference between HALOE and 14 midlatitude balloon correlative measurements of HCl ranged between 8 and 19% throughout most of the stratosphere, and the HALOE mixing ratios usually were lower than the correlative measurements [*Russell et al.*, 1996]. In the 0.3-50 mb region the total CH_4 mixing ratio error is of the order of 15% [*Park et al.*, 1996].

2.5. ClO

Version 4 MLS ClO mixing ratios are compared to model results at 21, 46, and 100 hPa. The MLS instrument is discussed by *Barath et al.* [1993], and *Waters et al.* [1996] discuss the validation of version 3 ClO. Version 3 and 4 MLS ClO data were retrieved at 100, 46, 21, 10, 4.6, 2.2, 1.0, and 0.46 hPa. We only used MLS ClO data if the quality indicator sign was positive (i.e., the a priori was not the dominant influence in the retrieval).

The orbital geometry of UARS allowed MLS to obtain approximately 400 observations northward of 40° latitude each day. The local times and the solar zenith angles, however, varied throughout each day. Therefore the diurnal solar zenith angle dependence of atmospheric ClO complicates the direct comparison of model and observed ClO values. In addition, UARS underwent a yaw maneuver on December 27, 1995, so MLS did not observe poleward of 34° north latitude from December 27, 1995, to January 26, 1996, when UARS again viewed the northern polar regions.

Determinations of the error bars for the version 4 ClO mixing ratios are based upon the recommendations by L. Froidevaux et al. available at http://mls.jpl.nasa.gov. Random errors for individual profiles are 0.3, 0.4, and 1.0 ppbv and accuracies (1 sigma) are 0.1, 0.1, and 0.3 at 21, 46, and 100 hPa, respectively.

3. Three-Dimensional Model

Observational data are compared to three-dimensional transport-chemical model values at 21, 31, 46, 68, and 100 hPa. The three-dimensional transport-chemical model, called ROSE, is similar to that described and applied by *Brasseur et al.* [1997]. The model is run on pressure coordinates between 316 and 0.31 hPa, in 37 equal divisions of log pressure, with a latitude spacing of 5° from 87.5°S to 87.5°N, and a longitudinal increment of 5.6°. UKMO temperature and wind fields [*Swinbank and O'Neill*, 1994] drive the model.

Gas phase chemistry is specified for 106 two and three body reactions, and 31 photolysis reactions. *DeMore et al.* [1997] two and three body reaction rates are used. There are 14 short lifetime species (e.g., $O(^3P)$, O_3, ClO, BrO) and 27 long-lifetime species (e.g., H_2O, CH_4, N_2O, HNO_3, HCl). The long-lifetime species concentrations change due to chemistry and are advected by application of the *Smolarkiewicz and Rasch* [1991] semi-Lagrangian formulation. The time step is 7.5 min. Photochemical equilibrium expressions are used to partition "chemical family" species into individual species concentrations.

The model is initialized with two-dimensional model mixing ratio fields [*Brasseur et al.*, 1990] and MLS mixing ratio fields of O_3. Table 1 specifies initial values of vortex averaged Cl_y (ClO + Cl +OClO + $2Cl_2O_2$ + $2Cl_2$ + HOCl + $ClNO_2$ + HCl + $ClONO_2$ + BrCl), HCl, $ClONO_2$, Br_y (BrO + HBr + $BrONO_2$ + HOBr, + Br + BrCl), and $BrONO_2$. The aerosol area densities are initialized with the SAGE two-dimensional climatological aerosol distribution displayed by *World Meteorological Organization (WMO)* [1991, Figures 3-5], multiplied by a factor of 0.60. The multiplicative factor of 0.60 was used to normalize the sulfate aerosol area densities to those inferred from the POAM II observations for positions both inside and outside the polar vortex during the first 12 days of the model simulations. The need for a multiplicative factor is not surprising, since the sulfate aerosol loading varies by a factor of 100 between background conditions and those shortly after a major volcanic eruption.

The model uses the six heterogeneous reactions for sulfate aerosol particles, the five heterogeneous reactions for Type I PSCs, and the five heterogeneous reactions for Type II PSCs, as cited by *Brasseur et al.* [1997, Tables 2b and 2a]. These reactions are

$$ClONO_2 + H_2O(s) \rightarrow HOCl + HNO_3, \quad (1)$$

$$ClONO_2 + HCl(s) \rightarrow Cl_2 + HNO_3, \quad (2)$$

Table 1. Initial Values of Vortex Averaged Chlorine and Bromine Reservoirs, and the Correspondence Between Pressure and Potential Temperature (θ) for Average Vortex Temperature Values

Pressure, hPa	θ, K	Cl_y, ppbv	HCl, ppbv	$ClONO_2$, ppbv	Br_y, pptv	$BrONO_2$, pptv
21	603	3.1	2.2	0.8	17	12
31	545	2.9	2.1	0.8	16	11
46	494	2.6	1.8	0.6	14	8
68	453	2.1	1.5	0.5	11	5
100	415	1.4	1.1	0.3	8	3

$$N_2O_5 + H_2O(s) \rightarrow 2HNO_3, \quad (3)$$

$$N_2O_5 + HCl(s) \rightarrow ClNO_2 + HNO_3, \quad (4)$$

$$HOCl + HCl(s) \rightarrow Cl_2 + H_2O, \quad (5)$$

$$BrONO_2 + H_2O(s) \rightarrow Cl_2 + HNO_3, \quad (6)$$

$$HOBr + HCl(s) \rightarrow BrCl + H_2O. \quad (7)$$

The (s) symbol refers to a species which is incorporated in the aerosol particle. Reaction probabilities for each reaction are specified for each type of particle composition (i.e., sulfate, nitric acid trihydrate (NAT), ternary, and ice) and follow, except for the cases discussed below, the recommendations of *DeMore et al.* [1997].

Model runs are carried out for the following cases: (1) only gas phase reactions are active, (2) gas phase and heterogeneous reactions on sulfate aerosol droplets are active, (3) gas phase and heterogeneous reactions on sulfate and ternary droplets are active, and (4) gas phase and heterogeneous reactions on both sulfate and NAT particles are active. For case (2) the aerosol area densities do not increase as temperatures drop below 195 K (i.e., high extinction PSCs are excluded from this calculation). For case (3) the area densities increase with decreasing temperature as specified by the aerosol physical chemistry model (APCM) model of *Tabazadeh et al.* [1994]. For case (4) the NAT area density is calculated according to the microphysical model of *Chipperfield et al.* [1993].

The reaction probabilities (γ) on sulfate (H_2O/H_2SO_4), NAT, and ternary droplets have been revised during the last several years. For example, the reaction probability for reaction (2) at 195 K at a pressure of 46 hPa and 5 ppmv H_2O has been revised from 3.2×10^{-3} [*Hanson et al.*, 1994] to 3.6×10^{-2} [*Hanson and Ravishankara.*, 1994, *Hanson*, 1998]. The newer formulation has a steeper temperature dependence than the original *Hanson et al.* [1994a] formulation. The differences in the reaction probabilities are due to new values of the water activity and HCl solubility in solutions containing < 50% wt H_2SO_4 [*Hanson*, 1998]. This increase in the reaction probability prompted *Ravishankara and Hanson* [1996] to note that heterogeneous reactions on sulfate can proceed at a rate comparable to that over solid Type I PSCs. The *Hanson* [1998] laboratory measurements also demonstrated that the presence of HNO_3 in a sulfate droplet lowers the reaction probability by a factor of 0.5.

Model calculations are carried out using both the *Hanson et al.* [1994] and *Hanson* [1998] reaction probabilities for reactions (1) and (2) on sulfate particles. *Donaldson et al.* [1997] reaction probabilities are utilized for reaction (5) on sulfate particles. The sulfate version of reaction (3) is given a constant value of 0.09 (i.e., the slight temperature dependence cited by *DeMore et al.* [1997] is not incorporated in the model).

In addition to the reactions utilized by *Brasseur et al.* [1997], the pathways

$$OH + ClO \rightarrow HCl + O_2 \text{ (4\% yield)}, \quad (8)$$

$$HO_2 + ClO \rightarrow HCl + O_3 \text{ (4\% yield)}, \quad (9)$$

and

$$OH + BrO \rightarrow HBr + O_2 \text{ (2.5\% yield)} \quad (10)$$

are used in the model. Model calculations are also carried out without these pathways.

Pathway (8) is discussed in terms of midlatitude photochemistry by *McElroy and Salawitch* [1989] and *Michelsen et al.* [1996]. As discussed by *Santee et al.* [1996], pathway (8) has been shown to improve the agreement between photochemical models and observations of ClO, HCl, and O_3 in the upper stratosphere. *Chipperfield et al.* [1996] used HCl production branches (8) and (9), which improved agreement between model and HALOE HCl values for the Southern Hemisphere vortex for September 1992.

Reaction (8) HCl production rates are given by the laboratory measurements of *Kegley-Owen* [1998, private communication, 1999]. These production rates and those of *Kegley-Owen et al.* [1999] are 1 and 4% lower, respectively, than those of *Lipson et al.* [1999] between 200 and 220 K. The range of measured yields for reaction (9) are discussed by *DeMore et al.* [1997]. *Chartrand and McConnell* [1998] present observational evidence for the production of HBr by reaction (10).

4. Vortex Morphology

Model results are presented in this paper in stereographic contour maps and by line graphs of the time trends of vortex averages. The vortex average of a variable in a line graph is a geographical weighted average. The weight at a model grid point is zero if the model point is outside the vortex and is equal to the ratio of the model grid element geographical area divided by the total vortex area if the model point is inside the vortex. Regions inside and outside the vortex are determined from a simple analysis of the potential vorticity (PV) field for each day, calculated from the UKMO wind fields. Inspection of the daily PV fields at each pressure level suggested a value of the PV contour that marked the regions of largest PV gradients for each day of the 40-day simulation. As noted by *Deniel et al.* [1998], this procedure produces results fairly similar to those based on the *Nash et al.* [1996] technique. Inspection of the model N_2O and CH_4 fields confirmed that the vortex was delineated by the daily PV contour values.

Plate 1 and Figure 1 illustrate that photolysis reactions take place in a portion of the polar vortex during some portion of each day throughout December and January. This is important since chlorine, when tied up in the Cl_2O_2 dimer, does not destroy ozone. Photolysis is needed to convert Cl_2O_2 into reactive chlorine. Plate 1 (left) displays the PV field on December 5, 1995, at 21 hPa. As in each of the contour graphs, latitudes between 40° and 90°N are presented, and the Greenwich meridian is near the "3 o'clock" position. The polar vortex in Plate 1 is not circular and is not centered over the pole (see *Manney et al.* [1994, Figures 1 and 2] for other examples). Plate 1 (right) of the present paper indicates the region in the polar vortex for which the local noon time solar zenith angle is < 90° (i.e., the region in which light penetrates during the day). There is a collar region in the vortex for the full range of days simulated by the model, for which the local noon time solar zenith angle is less than 90°.

Figure 1 displays daily values of the geographical area within the vortex for which the local noon zenith angle is < 90°. Since the hemisphere geographical area is 2.5×10^8 km^2, the illuminated portion of the vortex is between 4 and 12%, and the full vortex is between 7 and 14%, of the full hemispherical area. It is therefore apparent that the illuminated region in the vortex at all pressure levels varies by ~ 50% over the 40 day simulation.

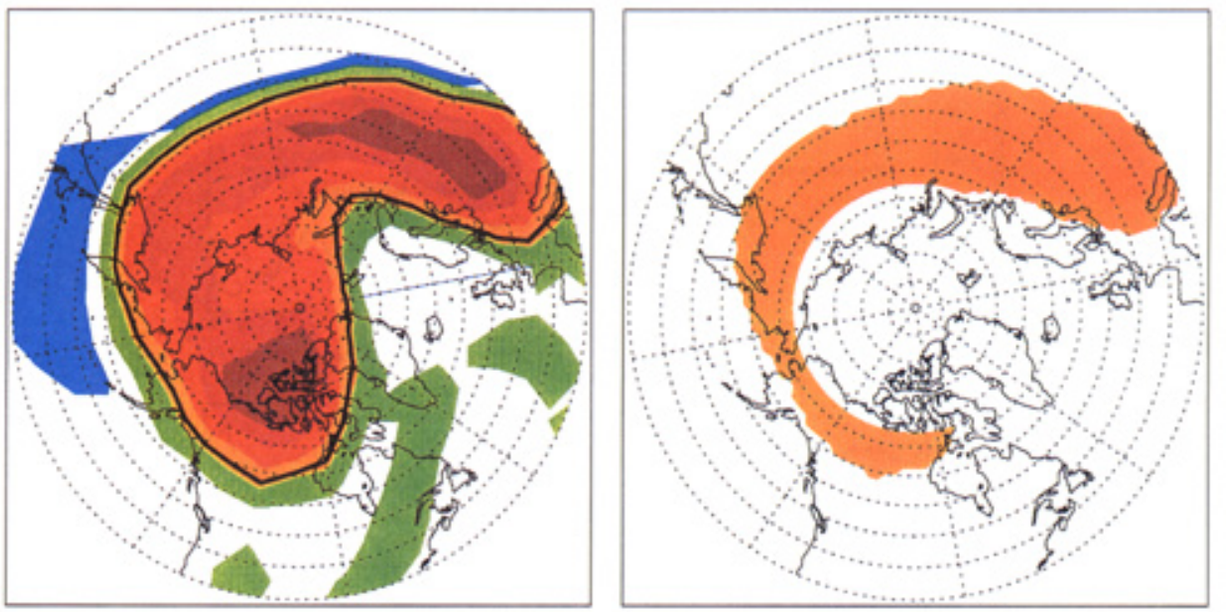

Plate 1. (left) UKMO potential vorticity values at 21 hPa for December 5, 1995. The heavy line marks the vortex boundary. (right) The area within the vortex which has a solar zenith angle less than 90° at local noon (i.e., sunlight is present during the day) is marked by the tan region

The values presented in Plate 1 and Figure 1 can be placed within a larger context by reference to the climatology of the vortex geometry calculated by *Waugh and Randel* [1999]. Waugh and Randel used elliptical diagnostics to calculate the area, center, elongation, and orientation of the Arctic and Antarctic stratospheric polar vortices for 1978-1998. At 490 K, which corresponds approximately to the 46 hPa surface, the average vortex geographical area is 1.6×10^7 km^2 for January [*Waugh and Randel*, 1999, Figure 3], while the January 1996 vortex area is approximately twice as large. The 1995-1996 northern polar vortex at 500 K is among the largest in the 1978-1998 time period, though the vortex elongation is close to the climatological average (W. Randel, personal communication, 1998).

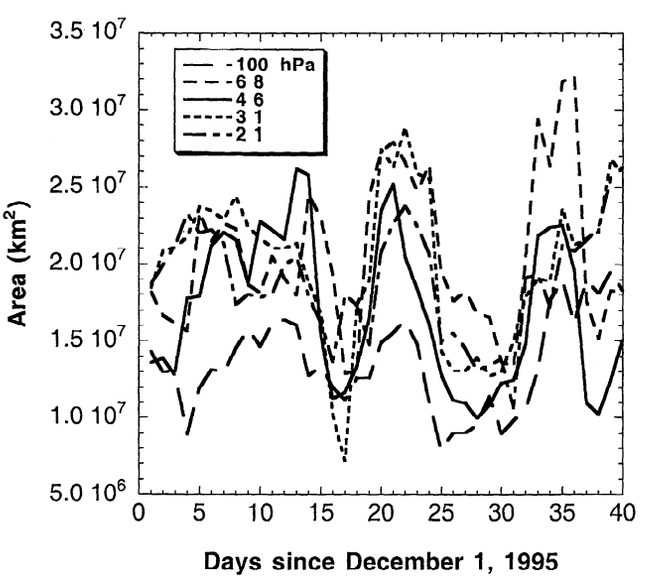

Figure 1. Geographical areas within the polar vortex which have solar zenith angles at local noon less than 90° at 21, 31, 46, 68, and 100 hPa.

5. Vortex Temperatures and Heterogeneous Reaction Rates

Gas phase and heterogeneous chemistry are dependent upon temperature. In this section we examine temperature trends inside the vortex, compare radiosonde temperatures to the UKMO values, and illustrate the temperature sensitivity of the heterogeneous chemistry reaction probabilities to model temperature biases.

The effective first-order rate constant (s^{-1}) for heterogeneous reactions is expressed as

$$k = 10^{-8}\ \gamma\ \ A\ \ v/4 \qquad (11)$$

where γ is the reaction probability (unitless) of the heterogeneous reaction, A is the aerosol area density (micron^2 cm^{-3}), and v is the mean molecular speed (cm/s). The area density A increases with decreasing temperature when ternary, NAT, or PSC II (ice) particles form. The value of γ also increases for reactions (1), (2), and (5) as temperatures decrease.

Figure 2 displays daily vortex averaged temperatures and the minimum temperature within the vortex for each day. The average temperatures are of the order of 200, 202, 205, 212, and 215 K at 21, 31, 46, 68, and 100 hPa, respectively, and the minimum temperatures are usually 10 K colder. While the vortex average temperatures oscillate about a mean value at each pressure level, the minimum temperatures exhibit a downward trend. Minimum temperatures, however, only occur for a small fraction of the full vortex region (see Figure 3). For example, 10% of the vortex at 46 hPa is at a temperature between 200 and

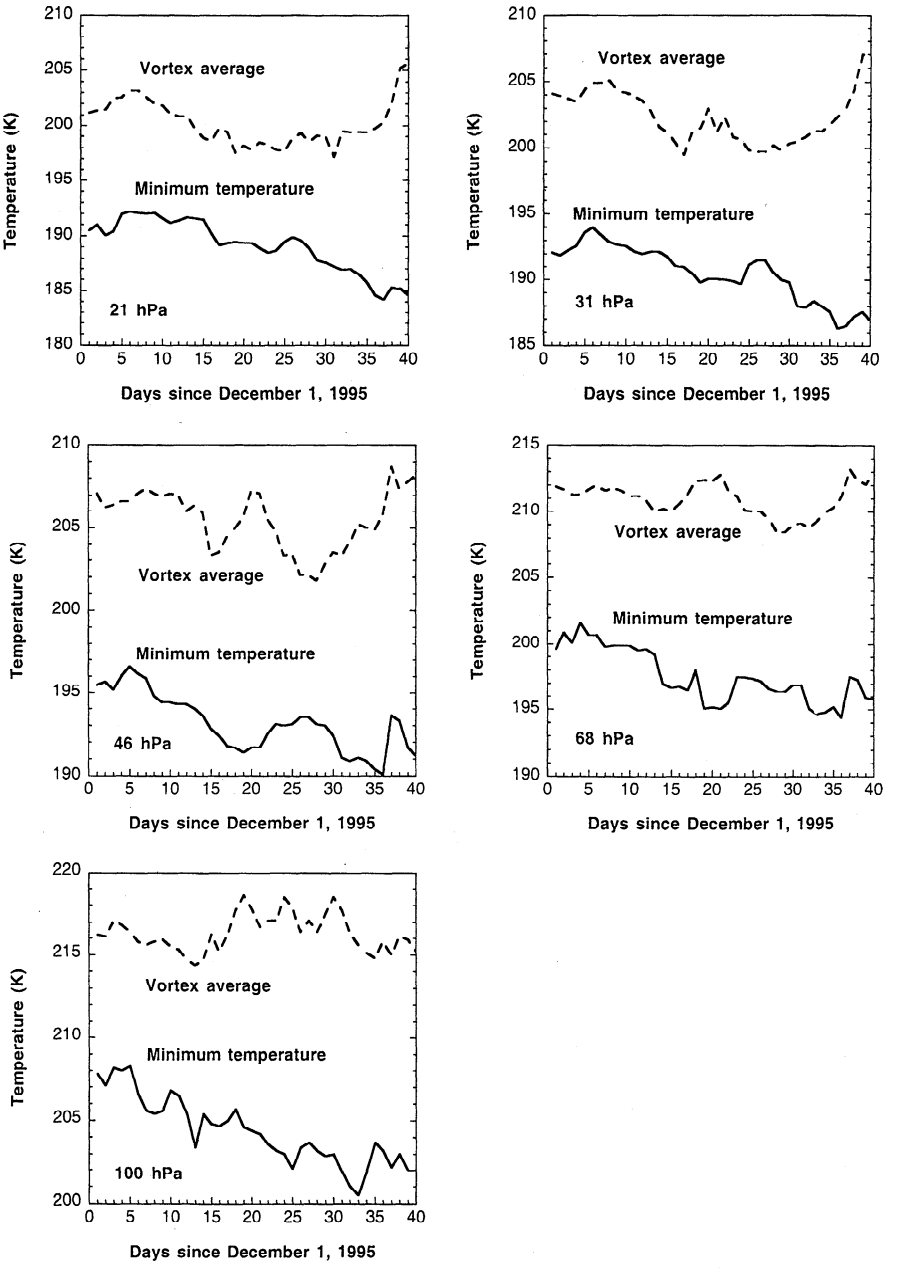

Figure 2. Vortex averages and minimum temperatures within the vortex for December 1, 1995, to January 9, 1996, at 21, 31, 46, 68, and 100 hPa.

202 K for days between December 6 and December 10, 1995, while only 4% is near 195 K. The geographical area fractions at the colder temperatures increase with time throughout December.

Coincident radiosonde temperatures were compared to the UKMO temperatures to assess the magnitude of the effect of model temperature biases on the heterogeneous chemistry reaction probabilities. Table 2 presents averages and standard deviations of the temperature differences ($T_{radiosonde} - T_{UKMO}$) for the time period December 1, 1995, to January 9, 1996. The average temperature bias is between –1.0 and –2.2 K for pressures between 100 and 21 hPa. A graph (not shown) of the temperature differences at 46 hPa, displayed as a function of $T_{radiosonde}$, shows that the -1.9 K average temperature difference at 46 hPa is representative for the full temperature range from 190 to 230 K.

Both the UKMO and National Center for Environmental Prediction (NCEP) temperature analyses show statistically significant differences from radiosonde data. *Manney et al.*, [1996, Table 1] cites UKMO temperature biases of -0.6, -1.0, -1.85, and -0.5 K for four 3-day periods between December 1994 and February 1995 for the Arctic between 36 and 54 hPa. Temperature differences (T_{sonde}-T_{UKMO}) of -1.7 and -1.6 K were calculated at 475 and 550 K for the 1994-1995 Arctic winter by *Pullen and Jones* [1997]. They note that errors in temperature analyses can lead to an underestimation of PSC area densities and that the timing of chlorine activation in model simulations may lag behind that of the real vortex.

A temperature decrease of 1 K increases the reaction probability by 24 and 38% at 46 hPa and 195 K for reactions (1) and (2), respectively. Since these sensitivities are fairly large, our

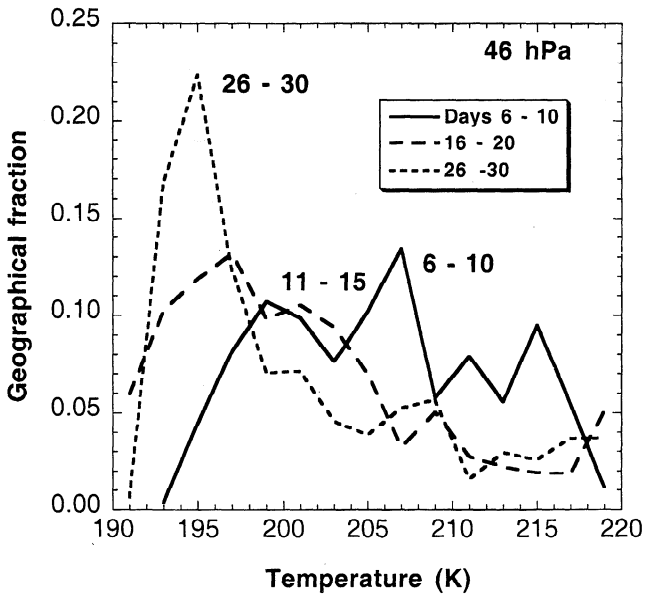

Figure 3. The distribution of temperature within the vortex at 46 hPa for December 6-10, December 11-15, and December 26-30, 1995.

model results likely underestimate the reaction probabilities for reactions (1) and (2) due to the UKMO temperature biases. In order to assess the sensitivity of ClO production to model temperature biases, a model calculation is carried out such that temperatures are decreased by 2 K at all pressure levels.

A further complication is due to the presence of gravity wave and mountain wave perturbations of temperature which are embedded in the larger-scale flow [*Carslaw et al.*, 1998]. Temperature perturbations of up to 15 K are possible over mountainous regions. These perturbations can locally alter reaction probabilities and aerosol composition, which enhances chlorine activation and ozone depletion. Such processes are not included in the present study.

6. Aerosol Area Density Distributions

POAM II extinction data at 1.06 μm were transformed into surface area densities using equation (5) of *Massie et al.* [1998] and the "average" transformation coefficients of *Massie et al.* [1998, Tables 4-6] for the time period from December 1, 1995, through January 9, 1996, at 21, 31, 46, 68, and 100 hPa. Data points for locations inside and outside the vortex are displayed in Figure 4, which also presents area density values calculated using the *Carslaw et al.* [1995] microphysical model for ternary droplets and the thermodynamic data of *Worsnop et al.* [1993] for NAT particles. Table 3 lists the inputs used in the theoretical equilibrium calculations. Values of H_2O are based upon 6-day averages of MLS version 4 data for January 1-7, 1992, and January 1-7, 1993, for latitudes greater than 60°N. The HNO_3 values are based on averages of MLS version 4 data for January 1992 and January 1993.

Theoretical temperature thresholds for NAT formation at 100, 68, 46, 31, and 21 hPa in Figure 4 are 196, 195, 194, 192, and 190 K, respectively. In Figure 2 the minimum temperatures are 200, 195, 190, 186, and 185 K at the five pressure levels. Therefore temperatures at 100 hPa are not cold enough for PSCs to form, while temperatures are cold enough for NAT particles to form at 68, 46, 31, and 21 hPa.

At all pressure levels there is an appreciable scatter of the sulfate area density values at temperatures above that of the NAT threshold. While some of this variation is likely due to limitations of the transformation coefficients and limitations due to the space view, i.e., a patchy aerosol field is interpreted by the inversion algorithm as a continuous distribution of aerosol along the observation ray path, a portion of the variation is real. This assertion is supported by in situ data. *Massie et al.* [1998, Figure 1] displays in situ forward scattering spectrometer probe (FSSP-300) area densities, and there is a factor of three variation in the area density at temperatures between 193 and 200 K for pressures between 50 and 60 hPa.

There are POAM II data points in Figure 4 which are larger than the model values by up to 3° above the theoretical NAT temperature threshold. For example, near 194 K at 21 hPa there are data points with area densities near 0.6 micron^2 cm^{-3} which lie to the right of the NAT curve. These points may be consistent with the NAT curve, owing to the differences ($T_{\text{radiosonde}} - T_{\text{UKMO}}$) discussed in section 5.

Overall, the model and the observations both display an increase in area density as temperatures decrease. PSCs are apparent for area densities greater than 0.4, 0.5, and 1.0 micron^2 cm^{-3} at 21, 31, and 46 hPa. The PSC data points are closer to the NAT curves than to the ternary curves.

Figure 5 displays daily averaged model and observed area densities. Model values are presented for the gas + sulfate, gas + sulfate + NAT, and gas + sulfate + ternary cases. The daily averages were calculated with colocated data (i.e., POAM values were compared to model values at the same latitudes and longitudes), and the averages were weighted by the geographical area of each grid point both inside and outside the vortex. At 100 and 68 hPa the values for the three model cases are identical since temperatures were at or above the NAT and ternary thresholds.

The error bars are calculated from the equation

$$e = (e_1^2 + (e_2/\sqrt{N})^2)^{1/2}, \quad (11)$$

where N is the number of observations used to form the average, e_1 is the measurement accuracy, and e_2 is the random error. A value of 30% is calculated for N=16, e_1=30% and e_2=15%. Averages in Figure 5 (and the other figures) have error bars which are dominated by systematic errors, since the number of observations reduces the random components substantially.

Since the latitude coverage of POAM II was between 63° and 65°N, the averaging process used to create Figure 5 does not sample the full vortex. Examination of contour graphs of model

Table 2. Average and Standard Deviations Between Radiosonde and UKMO Temperature Values for December 1, 1995, to January 9, 1996

Pressure, hPa	T_{sonde}-T_{UKMO}, K	σ, K
21	-2.24	4.85
31	-2.05	5.46
46	-1.88	2.41
68	-1.27	2.49
100	-0.99	2.45

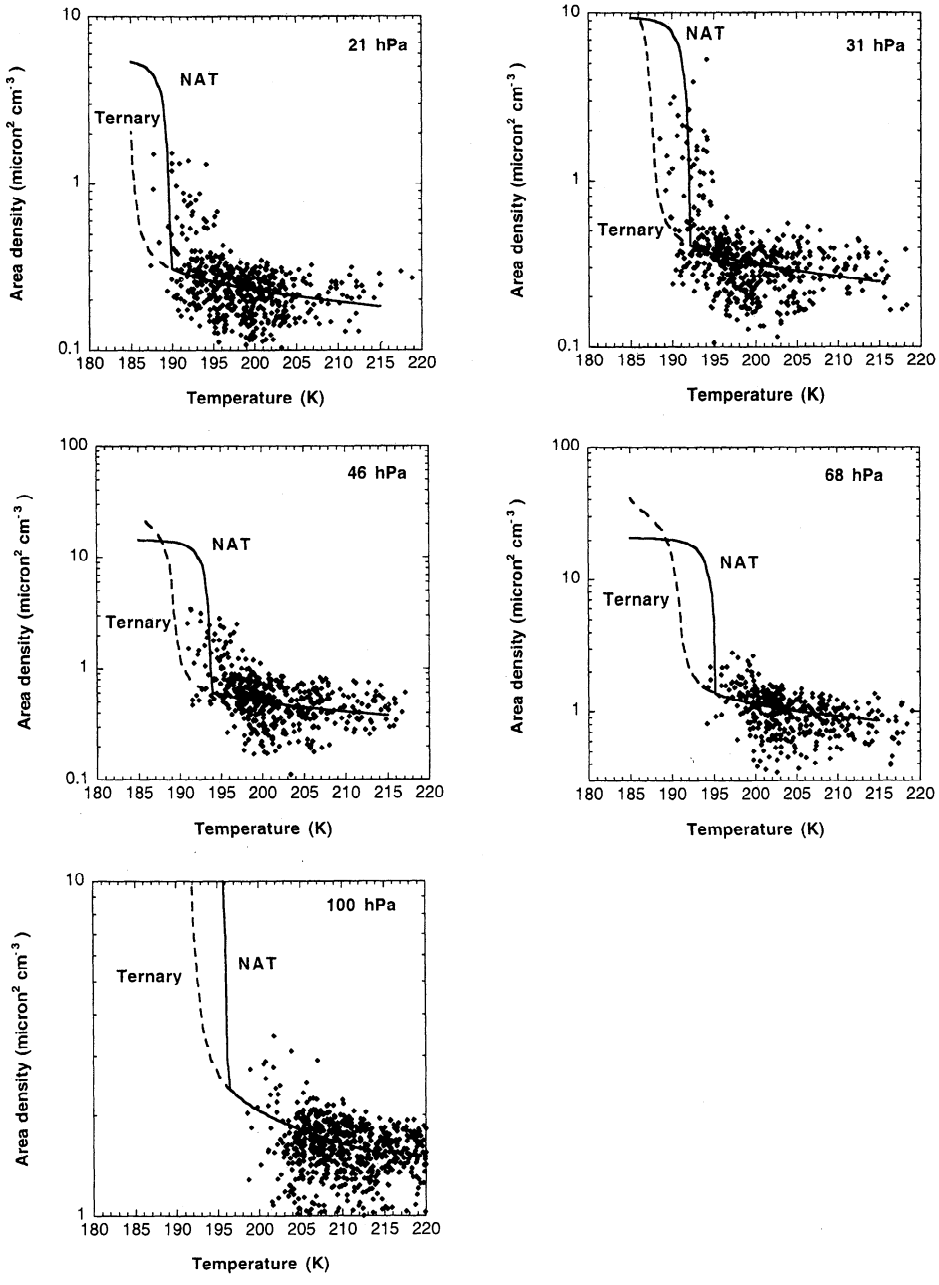

Figure 4. Comparison of POAM II area density values with NAT and ternary model values at 21, 31, 46, 68, and 100 hPa. Data points are both inside and outside the polar vortex and poleward of 40° latitude.

temperatures and area densities shows that the location of the coldest temperatures and largest area densities can be over the North Pole, such as on December 15. The dates of the peak aerosol densities in Figure 5 and the dates of the peaks in the time trends of the model vortex averaged area density (not shown), however, are very similar.

Figure 5 demonstrates that sulfate is the predominant aerosol during the first two weeks of December. On days 20 and 35 (December 20, 1995, and January 4, 1996) there are peaks in the model daily averages at 46, 31, and 21 hPa due to the development of PSCs. These peaks correspond to the dips in the minimum temperature curves of Figure 2. Temperature has a substantial influence on the area density as is evident from inspection of the model and POAM observations presented in Figure 4.

Figure 5 also reveals noticeable differences between model and observation. At 31 and 46 hPa the model values (for the gas + sulfate + NAT case) are larger than the observations and peak sooner than the POAM values.

At 68 hPa the POAM values display a larger variation in the daily averages than the model values. These differences may be due in part to temperature uncertainties in the UKMO temperature field. Figure 6 presents a comparison of daily averaged observed and model area density values (for NAT and sulfate particles) at 68 hPa for the standard model calculation of Figure 5 and one for which temperature values are decreased by 2

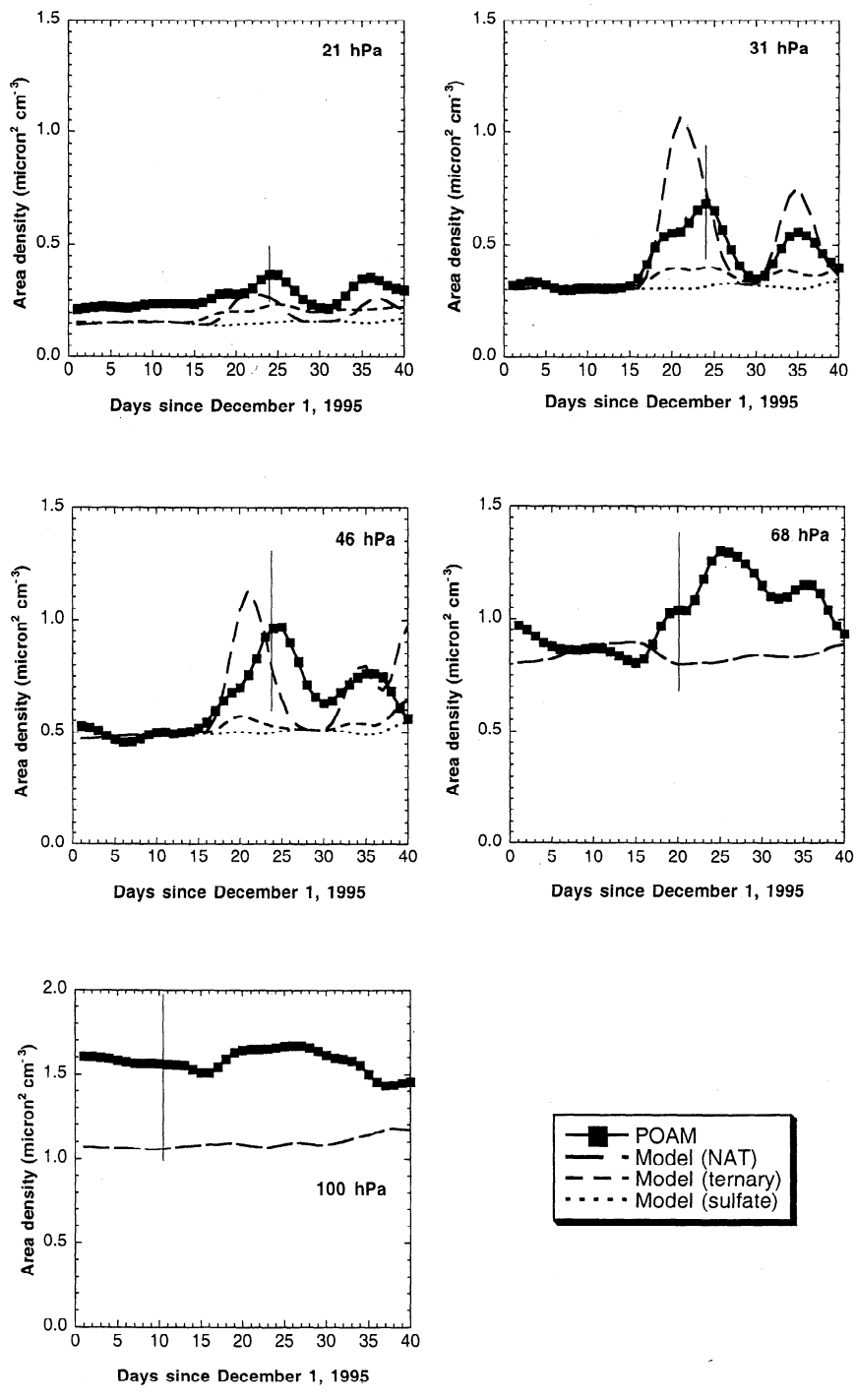

Figure 5. Daily averages of POAM II area density and model values at 21, 31, 46, 68, and 100 hPa. Averages are for inside and outside the vortex and poleward of 40° latitude.

K. The temperature decrease produces a noticeable increase in the area density values for days near day 20 and 35, since the minimum temperatures (see Figure 2) are near 195 K.

7. Model HCl

As noted in the introduction, the UKMO transformed Eulerian mean vertical wind field ($\overline{w^*}$) is positive, indicating a net upward component in the UKMO vertical motion field. The calculation time period of forty days in this study was therefore selected to lessen this problem. One way to assess the effects of this upward component on model mixing ratio fields of long lived species (such as HCl) is by examining model time trends of CH_4 and N_2O. CH_4 and N_2O mixing ratio profiles decrease with altitude, so that downward transport is expected to decrease the CH_4 and N_2O mixing ratios.

Table 4 presents model CH_4 and N_2O values and percent changes at the five pressure levels. For example, CH_4 averages change by +0.7% between days 36-40 (January 5 - 9, 1995) and 1-5 (December 1 - 5, 1995) at 46 hPa. The changes in CH_4 and

Table 3. Input Mixing Ratios for the Model Calculations of Figure 4

Pressure, hPa	H_2O, ppmv	HNO_3, ppbv
21	5.5	11
31	5.2	12
46	4.8	10
68	4.4	7
100	3.9	4

N_2O over a 40-day period for pressures between 68 and 46 hPa correspond to a vertical displacement of the mixing ratio profile of 0.7 km and an upwelling velocity of +0.02 cm s^{-1}. However, other calculations of $\overline{w^*}$ for the Arctic [*Schoeberl et al.*, 1992, Figure 5] yield a value near -0.07 cm s^{-1}. Though the upward vertical displacement of 0.7 km is not large over the 40-day period, the model wind field does not properly account for the downward transport of HCl from above. Since the influx of HCl is a source of active chlorine and this influx is not simulated by the model when UKMO winds are used, the model may underestimate the rate at which active chlorine is produced.

Table 5 presents model and HALOE observations of HCl as a check upon the model initialization of HCl. HALOE viewed at high latitudes in August and September 1995 and again in March 1996. The data in Table 5 are zonal averages between 65° and 75°N. The model and HALOE mixing ratios are within 0.2 ppbv at 21, 31, and 46 hPa, though the model values are 0.5 ppbv larger than the HALOE observations at 68 and 100 hPa, and the two sets of data are separated in time by three months. The comparisons at 68 and 100 hPa possibly indicate initial model values of HCl which are too large at these two pressure levels.

With these limitations in mind, Plate 2 examines the model distributions of HCl at 46 hPa. The blue regions in Plate 2 highlight areas for which HCl is less than 0.4 ppbv. The model predicts that HCl mixing ratios first decrease in a narrow band (Plate 2, upper left) on December 5, with mixing ratios near 1.2 ppbv, which are less than the vortex averaged values of 1.8 ppbv. This narrow band covers only a small portion of the polar vortex, and from Figure 5, this decrease occurs prior to the appearance of PSCs on December 20. By December 10 and December 15 there are localized patches of substantial HCl depletion with values near or less than 0.4 ppbv. By December 20 the area of depletion for which HCl is less than 0.4 ppbv has grown in size.

Time trends of vortex averaged HCl (not displayed) show that initial values of HCl are nearly constant during the first week of the model simulation, while the model displays a substantial decrease in N_2O_5. Vortex averages of model $ClONO_2$ are also fairly constant. $ClONO_2$ mixing ratios are approximately 1.0, 0.9, 0.7, 0.5, and 0.4 ppbv at 21, 31, 46, 68, and 100 hPa, respectively. The HCl and $ClONO_2$ time trends differ from the N_2O_5 time trends due to the temperature dependencies of reactions (1) – (3). The reaction probabilities for reactions (1) and (2) are highly temperature dependent, while that of reaction (3) is not.

Depletion of HCl also takes place outside of the polar vortex, since sulfate aerosol depletes HCl in the model simulations, and the sulfate is present both inside and outside the polar vortex. Validation of the model gas phase and heterogeneous chemistry requires comparisons of observed and model mixing ratios both inside and outside the vortex. Chemistry which produces agreement inside the vortex, yet produces disagreement outside the vortex, is incomplete.

Figure 7 presents observed HALOE HCl and model HCl mixing ratios at 46 hPa for latitudes greater than 30° north in order to compare model HCl values with observations both inside and outside the polar vortex. As noted in Section 2, the HALOE experiment just barely makes measurements within the polar vortex during the December - January time frame. The dark squares in Figure 7a are HALOE sunrise observations for model days 15 - 39 (December 15, 1995 to January 8, 1996), and the open squares are sunset observations for January 14 to February 1, 1996. HALOE sunrise observations were near 48°N latitude on December 25, and HALOE sunset observations were near 50°N latitude on January 24. In Figure 7a there are several points near 50°N where the mixing ratios are below 0.9 ppbv, which are assumed to indicate the location of chemical depletion of HCl in the vortex. In Figures 7b and 7c the model values, which correspond to observations on December 25 and 26, are presented with and without the HCl production pathways cited in equations (8), (9), and (10). Figure 7d presents the differences in the individual model values of Figure 7b and Figure 7c. If these production pathways are not included (see Figure 7c) in the model simulation, then the model overestimates the depletion of HCl at latitudes between 40° and 50°N. If the pathways are included (see Figure 7b), the model HCl values compare more favorably to the observations, though the depletion is still overestimated between 40° and 50°N.

8. Chlorine Activation

8.1. Contour Maps of Active Chlorine

Plate 3 presents mixing ratios of Cl_x ($ClO + 2Cl_2O_2 + Cl + OClO + 2Cl_2 + HOCl + ClNO_2$) at 46 hPa on December 5, 10,

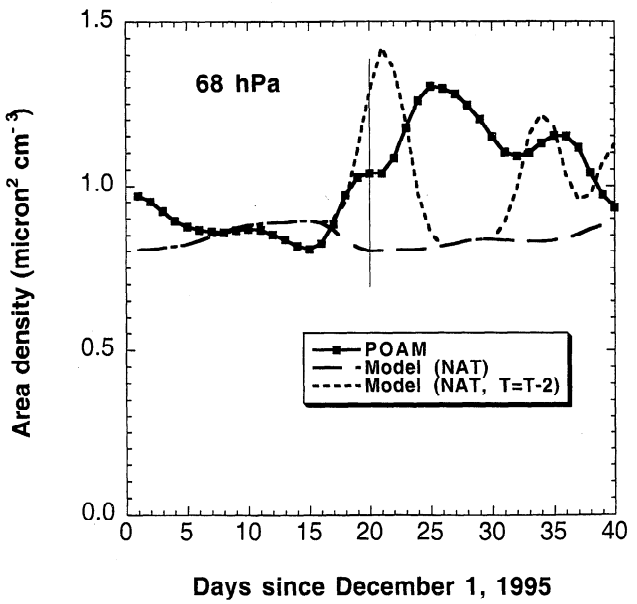

Figure 6. Daily averages of POAM II area density and model values at 68 hPa. Averages are for inside and outside the vortex, and poleward of 40° latitude. The model curves are for the case where sulfate and NAT particles are present. The long dashed curve is the same as in Figure 5, and the short dashed curve is for the model simulation in which temperatures are decreased by 2 K.

Table 4. CH_4 and N_2O Model Mixing Ratios, Inside and Outside the Vortex

Pressure, hPa	CH_4, outside		CH_4, inside		N_2O, outside		N_2O, inside	
	ppmv	%	ppmv	%	ppbv	%	ppbv	%
21	0.81	3.8	0.53	10.7	79	11.8	36	21.5
31	0.96	1.3	0.71	7.9	119	3.1	70	14.2
46	1.09	0.7	0.92	7.4	161	0.5	121	12.7
68	1.22	0.9	1.12	4.6	203	0.8	176	6.8
100	1.39	-0.6	1.28	2.3	240	-1.1	220	3.0

The mixing ratios are model averages for days 1-40. Percent change values are percent differences for the averages of days 36-40 and days 1-5.

15, and 20 to illustrate chlorine activation in the vortex. On December 5 the Cl_x is contained within the low latitude portion of the vortex and overlies the region of HCl depletion presented in Plate 2. On December 10 there are two portions of the vortex which have Cl_x values greater than 0.5 ppbv. The region of Cl_x greater than 1.6 ppbv is associated with the region of HCl in Plate 2 which is less than 0.4 ppbv. By December 20 a large portion of the vortex displays Cl_x greater than 1.6 ppbv, which clearly corresponds to regions of low HCl in Plate 2.

The model results suggest that active chlorine is not uniform within the vortex several weeks after the initialization of chlorine activation, although the distribution of chlorine activation is anticorrelated with that of the HCl displayed in Plate 2. These results are similar to those reported previously in other three-dimensional model studies. *Douglass et al.* [1993] and *Yudin et al.* [1997] both point out that sporadic polar processing initially takes place in the Arctic polar vortex before a "permanent" region of polar processing becomes established.

8.2. ClO Diurnal Variation

Figure 8 presents MLS version 4 ClO mixing ratios at 46 hPa for 6 days during December 19 - 25. The MLS experiment is viewing the Southern Hemisphere after December 25, so December 19 - 25 is the last available week in which to examine the development of ClO during the early chlorine activation phase. Negative mixing ratios in Figure 8a indicate the noise component of single MLS retrievals at 46 hPa. It is apparent from Figure 8a that ClO values are appreciably higher during the daytime. Model values of ClO (for the gas + sulfate + NAT case) are presented in Figure 8b. The model and MLS values both vary over a several ppbv range of mixing ratio. By averaging the MLS and model values in 2° bins of solar zenith angle, the MLS noise component is reduced substantially. Figure 8c presents these averages, and those from the model run. The diurnal cycle for both model and observation are fairly similar. Daytime averages are of the order of 0.6 to 0.8 ppbv, while nighttime values are less than 0.2 ppbv.

The increase in ClO as the solar zenith angle increases during the day is not interpreted as a real feature of the ClO diurnal cycle since there are meridional gradients in ClO and solar zenith angle. However; Figure 8 does show that there is a distinct difference between day and nighttime values of ClO and that both the model and observed ClO values are similar when graphed as a function of solar zenith angle. The nighttime values in Figure 8 also indicate that comparisons of averaged version 4 MLS ClO data with model values at the 0.2 ppbv level are meaningful.

Figure 8 supports the validity of the chemical framework used in this study, which requires that there is a strong diurnal cycle imposed upon ClO. If the nighttime MLS averages were substantially larger than the nighttime model values, then the chemistry would underestimate the production of active chlorine. This is not apparent from the results presented in Figure 8.

Other studies have also examined the diurnal variation of ClO. Figure 16 of *Waters et al.* [1996] shows the diurnal variations of ClO during August 14-29, 1992, over the Antarctic vortex at 21, 46, and 100 hPa. Averages of observations in which ClO at 46 hPa was at maximum yield a diurnal variation in which ClO is near 2.3 ppbv for zenith angles near 80° and near 0.1 ppbv for zenith angles greater than 90°.

8.3. Five Day Averages of ClO

Five day averages of MLS ClO at 21, 46, and 100 hPa and model ClO at 100, 68, 46, 31, and 21 hPa are presented in Figures 9-12. Five-day averages were calculated in order to

Table 5. HALOE and Model HCl Zonal Averages

Pressure, hPa	HALOE, ppbv		Model, ppbv
	sunrise	sunset	
21	2.1	2.3	2.1
31	1.8	2.1	2.0
46	1.5	1.6	1.7
68	1.1	1.1	1.5
100	0.6	0.6	1.1

The sunrise and sunset observations are from August and September 1995. The model values are for December 5, 1995, and all zonal averages are for latitudes between 65° and 75°north.

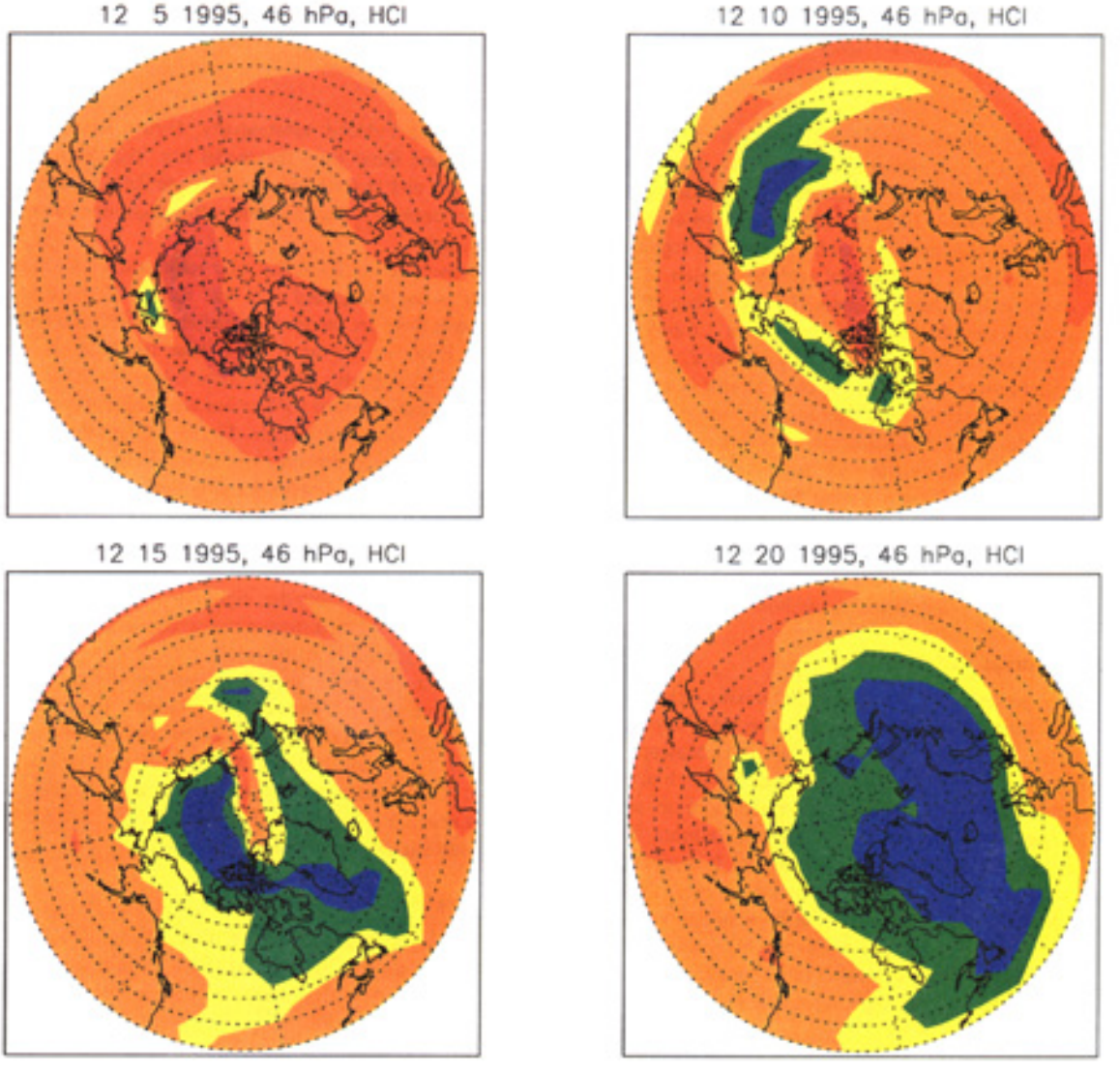

Plate 2. Contour graphs of model HCl (ppbv) at 46 hPa for December 5, 10, 15, and 20, 1995. Model values for gas + sulfate + NAT chemistry are displayed. Regions for which the HCl is less than or equal to 0.4 ppbv are indicated by the blue portions of the graphs.

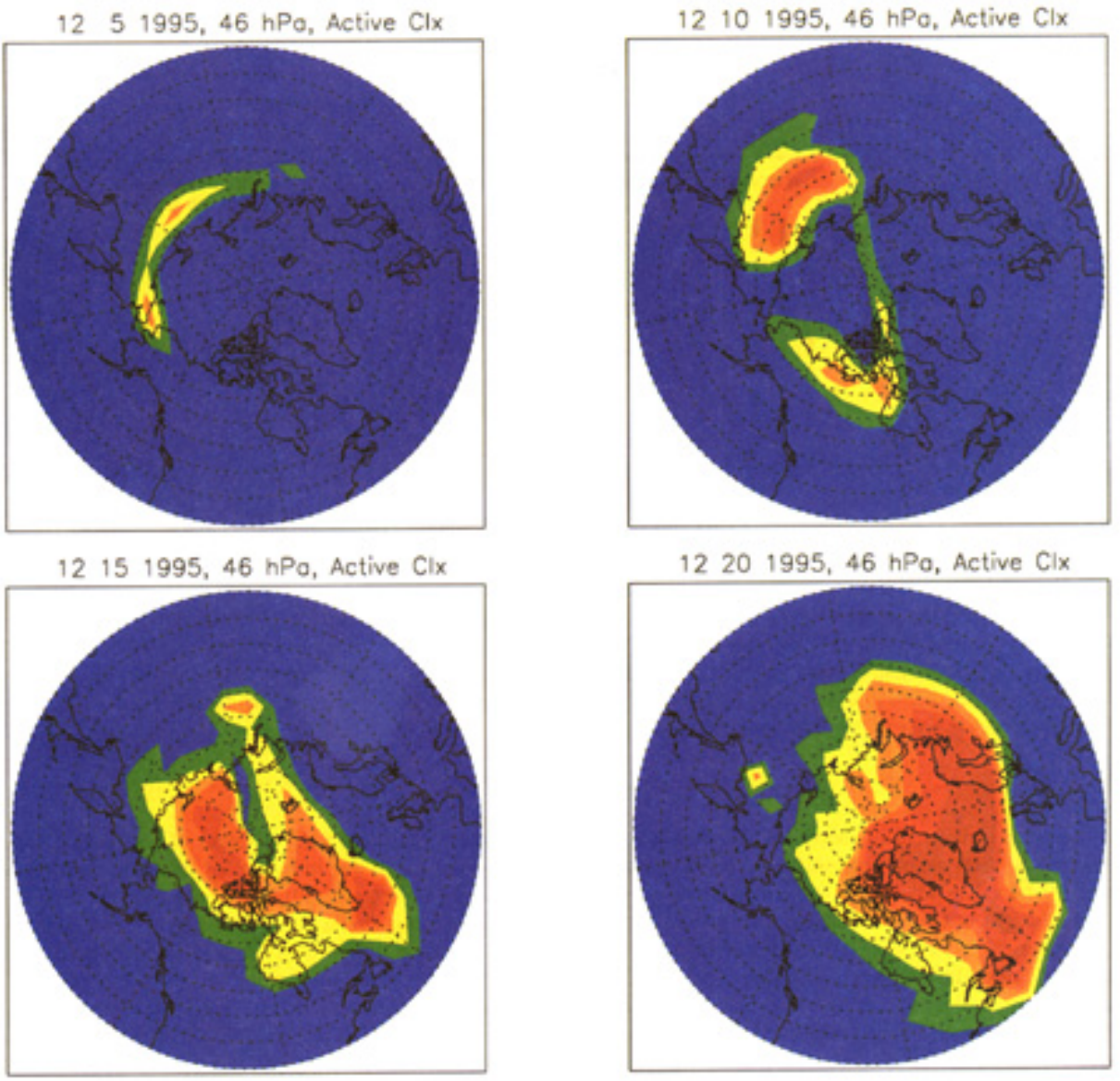

Plate 3. Contour graphs of model Cl_χ ($ClO + 2Cl_2O_2 + Cl + OClO + 2Cl_2 + HOCl + ClNO_2$) (ppbv) at 46 hPa for December 5, 10, 15, and 20, 1995. Model values for the gas + sulfate + NAT chemistry are displayed. Regions for which the active chlorine is greater than 1.6 ppbv correspond to the regions in Plate 2 for which HCl is less than 0.4 ppbv.

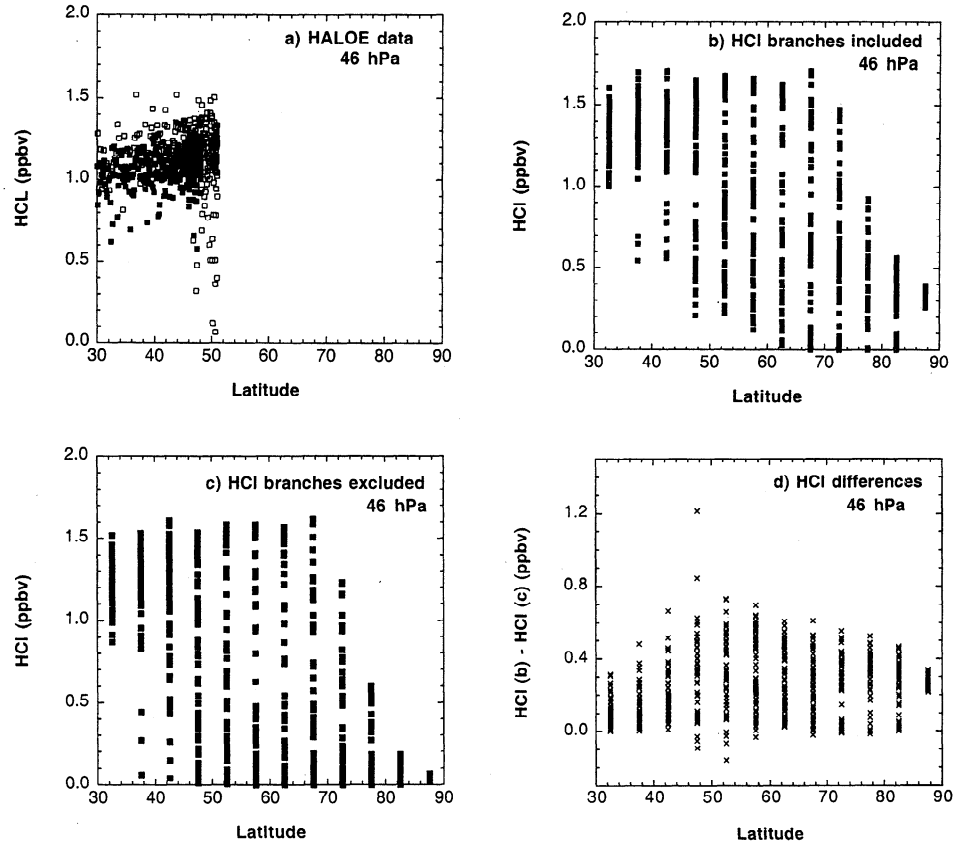

Figure 7. (a) HALOE HCl (ppbv) mixing ratios at 46 hPa for December 14, 1995 through January 9, 1996, are denoted by the solid squares. The open squares mark the observations for January 14 through February 1 (which would correspond to model days 45-63). The vortex is sampled slightly near latitude 50°N. (b) Model HCl (ppbv) mixing ratios at 46 hPa for December 25-26, 1995, the days when HALOE made observations near 48°N. Reaction pathways (8), (9), and (10) are included in the model calculations. (c) Model HCl (ppbv) mixing ratios at 46 hPa for December 25-26, 1995. Reaction pathways (8), (9), and (10) are excluded from the model calculations. (d) Differences in ppbv of the individual HCl values from Figures 7b and 7c.

reduce the noise component of individual values. MLS values were used if the solar zenith angle of the observation was less than 90°. Model values were used, at the model output times of noon and midnight at Greenwich, if the solar zenith angle was also less than 90°. The comparisons therefore are not for colocated positions. The number of coincidences was small when averages were calculated using colocated, simultaneous observations, and these averages contained a substantial noise component.

Error bars are calculated using equation (11) and the random and systematic errors cited in section 2.5. Since the number of observations is of the order of 80 for each daily average, the error bars are essentially due to systematic errors.

Figures 9-12 do not compare model maximum values with observed MLS maximum values. This type of comparison would be difficult owing to the noise inherent in individual MLS observations and owing to the limitations of the model output, which is programmed at 0 and 12 UT. Maximum values of Cl_x in Plate 3 at 46 hPa for days 15 and 20 are 2.4 and 3.1 ppbv, and maximum model ClO values (not shown) are 1.8 and 1.8 ppbv, respectively. Maximum values of ClO are therefore substantially larger than the vortex averaged values presented in Figures 9-12.

Figure 9 displays 5-day averages of ClO mixing ratio inside the vortex, and the influence of reaction probabilities and reactions (8), (9), and (10) are examined for the sulfate + NAT case. The open circles mark simulations in which the *Hanson* [1994] reaction probabilities are used without reactions (8)-(10). The triangles mark simulations in which the *Hanson* [1998] reaction probabilities are used, and the open squares mark simulations in which the *Hanson* [1998] reaction probabilities and reactions (8)-(10) are used. The model ClO values after day 25, especially at 46 and 31 hPa, are ~ 0.2 ppbv lower than the "older chemistry" model values when reactions (8)-(10) and the *Hanson* [1998] reaction probabilities are utilized. The *Hanson* [1998] reaction probabilities for reactions (1) and (2) have a steeper temperature dependence than the *Hanson et al.* [1994] reaction probabilities, so less active chlorine is produced at the average vortex temperatures displayed in Figure 2. Reaction pathways (8) and (9) increase HCl (see Figure 7) and decrease ClO in the vortex, especially at 31 and 46 hPa after December 25.

At 46 hPa the model and observed ClO averages increase with time in similar fashion. At 21 hPa the MLS average for simulation days 16-20 is larger than the model averages, though the comparison for days 21-25 is somewhat closer. At 100 hPa

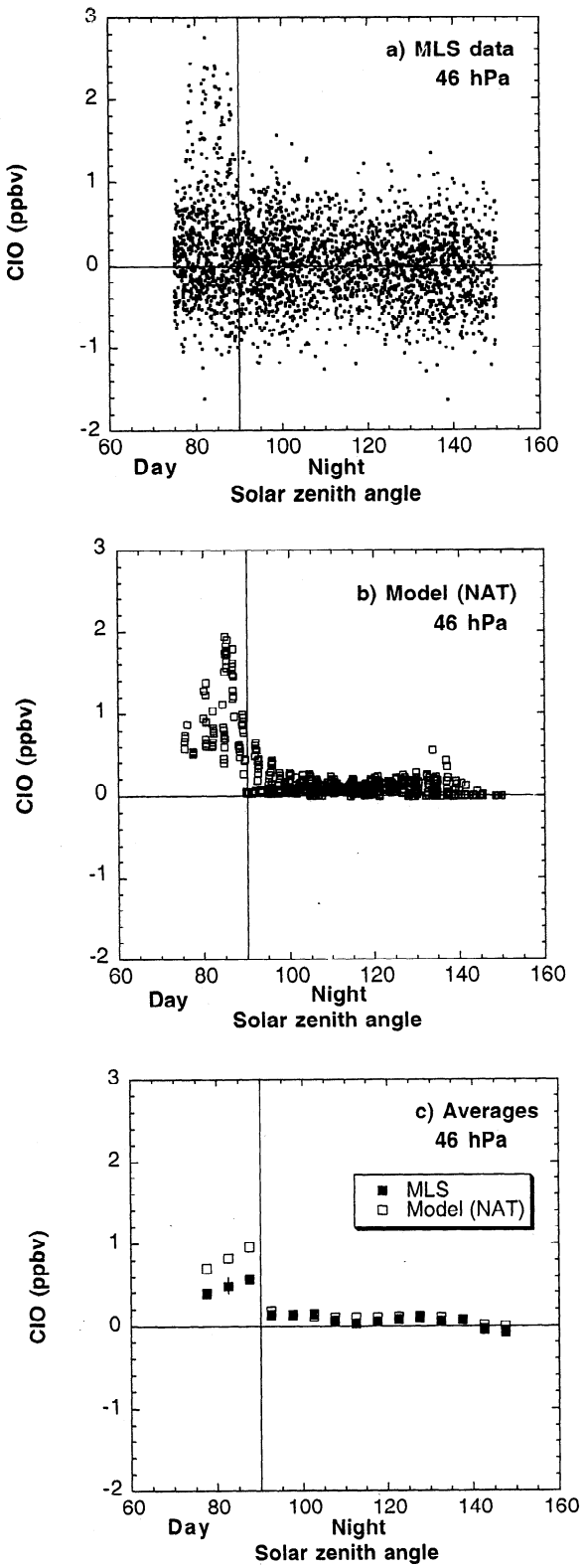

Figure 8. (a) MLS version 4 ClO (ppbv) within the vortex at 46 hPa for December 19 - 25, 1995. Negative mixing ratios are indicative of the noise level present in the MLS retrieval at this pressure level. (b) Model ClO values inside the vortex, for the gas + sulfate + NAT case, at 46 hPa for December 19 - 25, 1995. (c) Averages (2° bins of solar zenith angle) of MLS version 4 ClO (ppbv) within the vortex at 46 hPa for December 19-25, 1995, and averages of the model values. Model values for the gas + sulfate + NAT chemistry are displayed. All model and MLS data points within the vortex were used in the averaging process.

the comparison is problematic owing to the large MLS error bars.

Figure 10 presents the baseline case (gas + sulfate + NAT chemistry, reactions (8)-(10), and the *Hanson* [1998] reaction probabilities) and two sensitivity calculations. In section 5 it was noted that the UKMO temperatures are warmer than the radiosonde data by ~ 2 K between 21 and 46 hPa. If temperatures are uniformly reduced by 2 K at all pressure levels, then more ClO is produced (see the open circles in Figure 10), especially at 21 and 31 hPa. The temperature sensitivity is much less pronounced at 46, 68, and 100 hPa. The other sensitivity calculation in Figure 10 is given by the triangles, for the case where the sulfate aerosol has been reduced by 30% from the baseline case. As expected, the amount of ClO produced is reduced, by roughly 0.1 ppbv, between 31 and 68 hPa.

Figures 11 and 12 present 5-day averages inside and outside the vortex, respectively, for three cases: (1) gas + sulfate chemistry only (circles), (2) gas + sulfate + ternary chemistry (triangles), and (3) gas + sulfate + NAT chemistry (squares). For all three cases, reactions (8)-(10) and the *Hanson* [1998] reaction probabilities were utilized. At 46, 68, and 100 hPa the gas + sulfate chemistry alone provides the majority of the chlorine activation inside the vortex. This result is consistent with the conclusions of *Portmann et al.* [1996], who note that the long-term changes in the magnitude of the Antarctic ozone hole are modulated by variations in aerosol surface area connected to volcanic sulfate aerosol loading and that the sulfate aerosol is effective at converting chlorine from reservoir species to active forms.

At 21 and 31 hPa the presence of NAT PSCs substantially increases the production of ClO after day 15. The ternary case produces less chlorine activation than the sulfate case since, as noted in section 3, the *Hanson* [1998] laboratory measurements demonstrated that the presence of HNO_3 in a droplet lowers γ by a factor of 0.5. Outside the vortex, where there are fewer PSCs, the gas + sulfate case provides most of the chlorine activation at all pressure levels.

At 46 hPa the model and observed ClO mixing ratios increase with time in a similar fashion both inside (Figure 11) and outside (Figure 12) the vortex. At 21 hPa the time trends are fairly similar both inside and outside the vortex. Comparisons at 100 hPa are problematic due to the larger error bars of the MLS data at this pressure level. Overall, 11 of the 14 MLS averages in Figures 11 and 12 at 21 and 46 hPa have error bars which overlap with the gas + sulfate + NAT model values. Time trends of these 5-day averages of model and version 4 MLS ClO inside and outside the vortex at 21 and 46 hPa therefore agree within the experimental error.

In Figure 11, the amounts of chlorine activation inside the vortex at 21, 31, and 46 hPa for the NAT simulation are larger than that of the ternary simulation. This result is fairly similar to that reported by *Sessler et al.* [1996], who used box models and the SLIMCAT three-dimensional chemical transport model to study the chlorine activation and deactivation stages for the 1994/1995 Arctic winter. After a cold PSC event (T_{min} < 190 K), NAT and ternary cases produced similar amounts of chlorine activation on the 465 K potential temperature surface. For higher minimum temperatures, i.e., temperatures between the effective ternary and NAT thresholds, the NAT case yielded more chlorine activation. From Figures 2-5 it is apparent that the minimum temperatures for the December 1995 to January 1996 time period were between the effective ternary and NAT thresholds. These conditions produced more chlorine activation in the NAT simulation than in the ternary simulation.

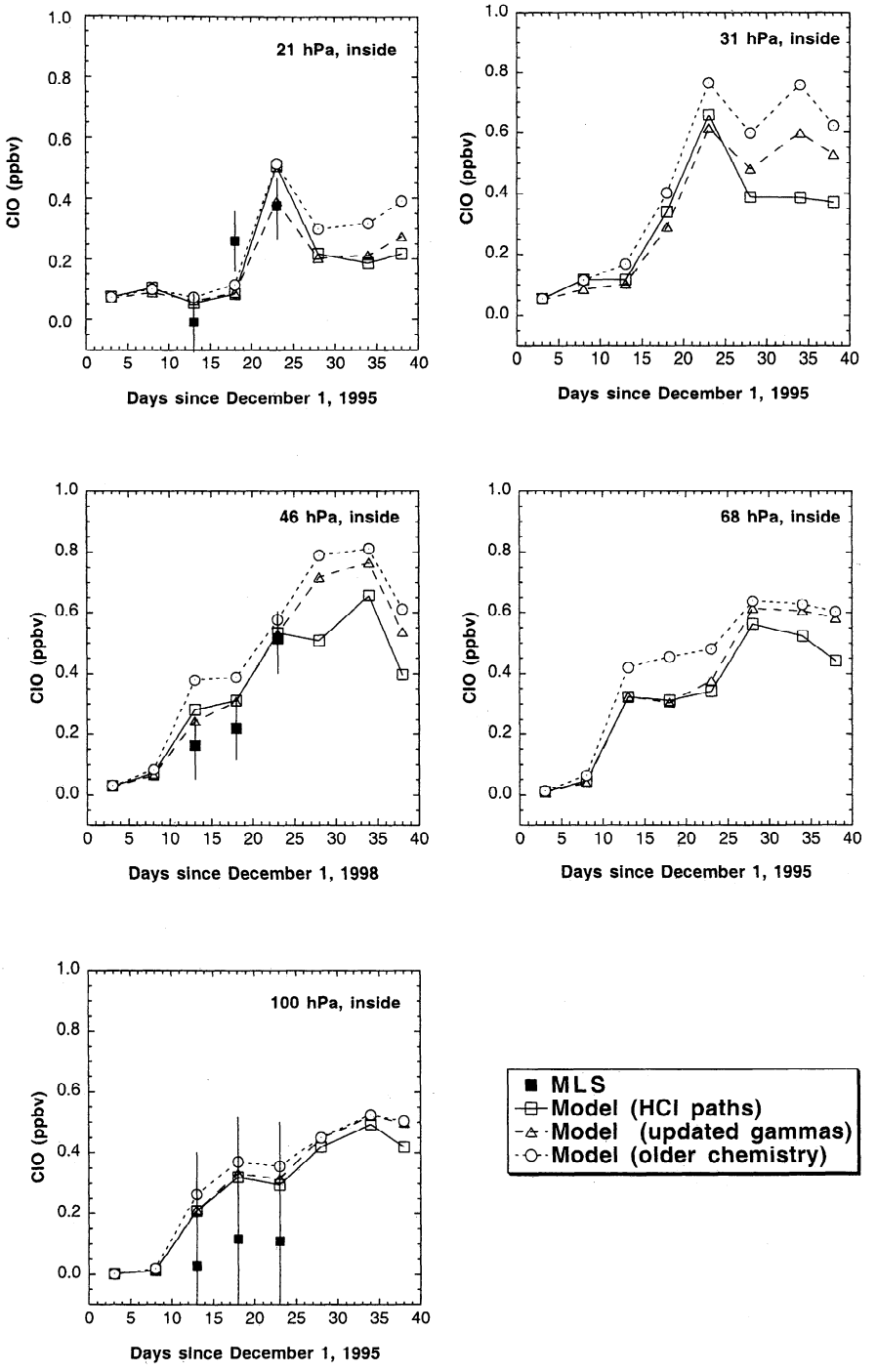

Figure 9. Five day averages of model and MLS ClO (ppbv) at 21, 46, and 100 hPa. The model values correspond to the gas + sulfate + NAT case. All model values and MLS data points within the vortex, at latitudes greater than 40°N, and for which the solar zenith angle was less than 90°, were used in the averaging process. UARS looked southward of 35°N after December 27, 1995. "Older chemistry" uses *Hanson et al.* [1994] reaction probabilities, "updated gammas" use *Hanson et al.* [1998] reaction probabilities, and "HCl paths" use the updated gammas and the HCl paths of reactions (8), (9), and (10).

9. Conclusions

Quantitative comparisons of observation and model results at each of the following cause and effect links, (1) temperature, (2) generation of aerosol area density, and (3) conversion of inactive chlorine to active chlorine, were carried out for the time period from December 1, 1995 through January 9, 1996. This time period was selected owing to the availability of UARS mixing ratios of HCl and ClO, POAM II aerosol extinction data, and because stratospheric temperatures were very cold.

Minimum temperatures reached down to 195 K at 46 hPa by December 7 (see Figure 2). The presence of cold temperatures was expected to enhance the surface area of aerosol because of the creation of PSCs. This link was examined by transforming

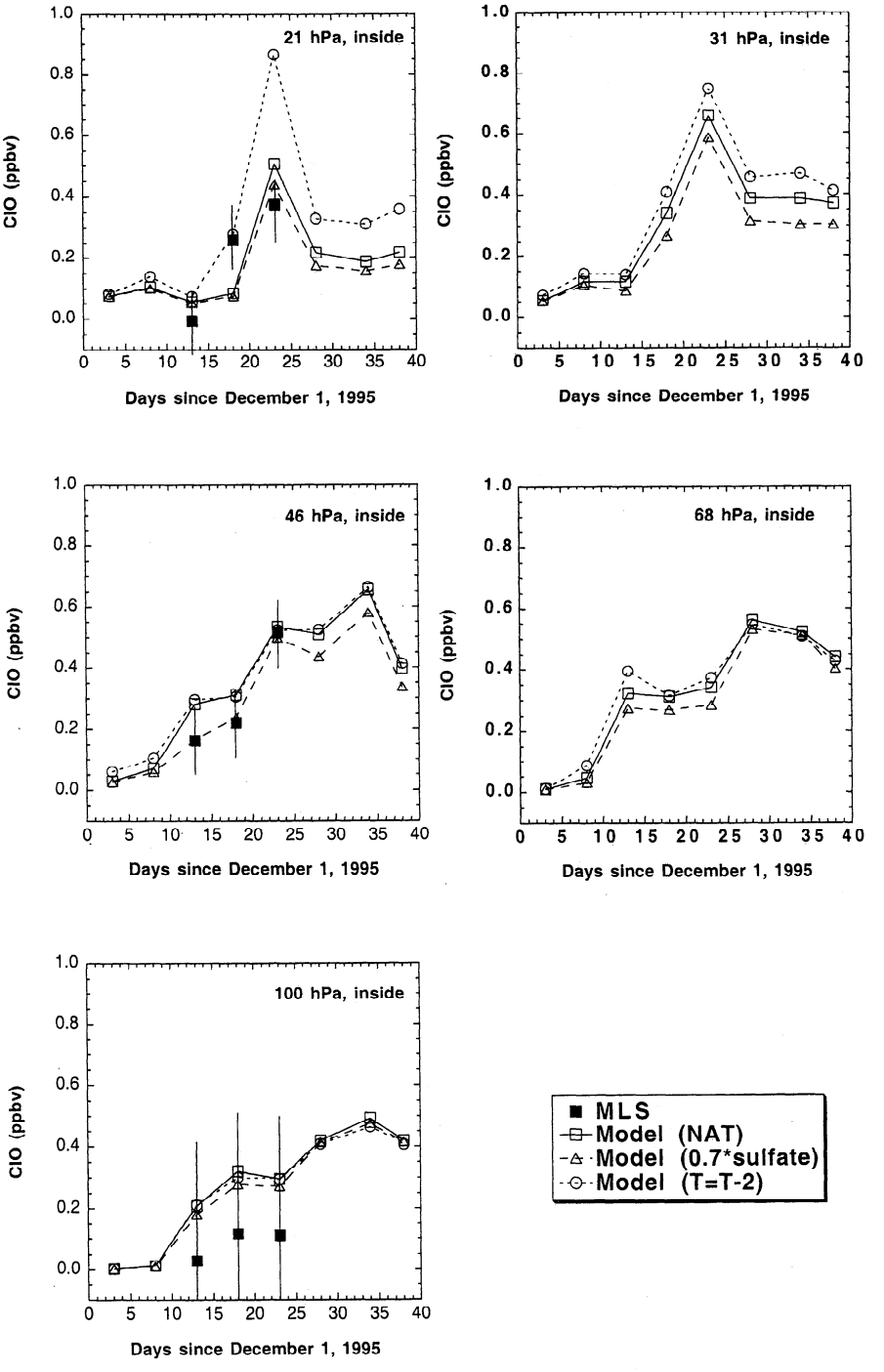

Figure 10. The averaging used is the same as in Figure 9. The "NAT" baseline case (open squares) uses the *Hanson et al.* [1998] reaction probabilities and the HCl paths of reactions (8), (9), and (10). The "0.7 sulfate" case (triangles) is based upon multiplying the sulfate aerosol density by 0.7. The "*T*=*T*-2" case (open circles) uses the baseline case chemistry and temperatures decreased by 2 K at all pressure levels.

POAM extinction data into area density values, which were compared to model calculations for sulfate, NAT, and ternary particles. PSC particles were observed in the POAM data at 46, 31, and 21 hPa. The POAM data matched the NAT model calculations better than the ternary model calculations (see Figure 4). Variations of daily aerosol density averages for model and observation at 31 and 46 hPa were in fair agreement (see Figure 5). As POAM averages increased, the model averages also increased. Model values at 31 and 46 hPa, however, peaked before the observed values, and the model values were larger than the observed values.

The cold temperatures in early December initiated the conversion of model unreactive chlorine (HCl and $ClONO_2$) into HOCl and Cl_2. The large geographical area of the northern polar vortex in December 1995 and January 1996 extended to latitudes far enough south, such that photolysis was active inside the polar vortex throughout December and January (see Plate 1).

Model calculations were carried out for four cases, (1) gas

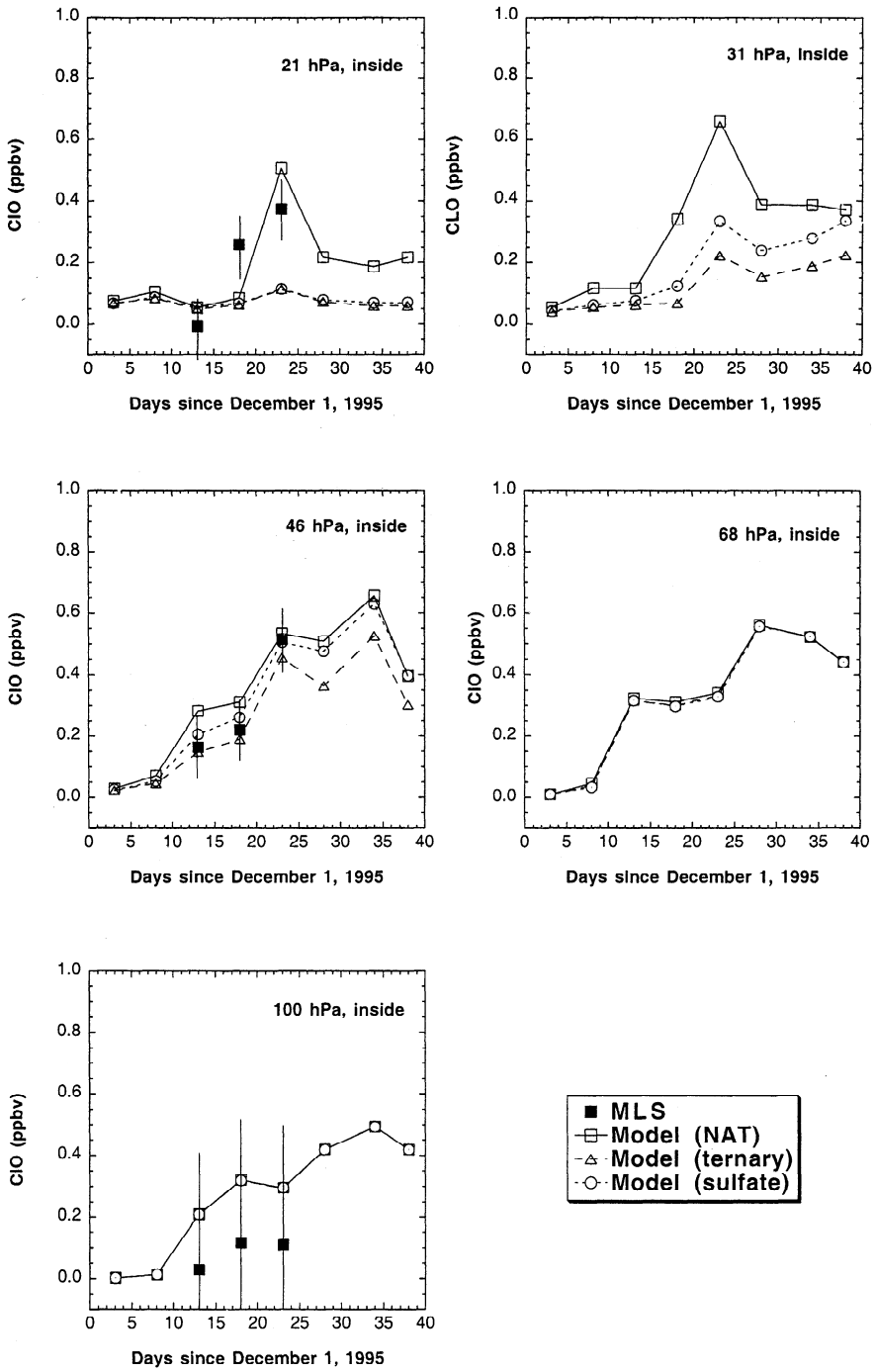

Figure 11. The averaging used is the same as in Figure 9. "NAT" model values are for gas + sulfate + NAT reactions, *Hanson et al.* [1998] reaction probabilities, and the HCl paths of reactions (8), (9),and (10). "Ternary" values are for gas + sulfate + ternary reactions, and "sulfate" values are for the gas + sulfate reactions.

phase reactions only, (2) gas + sulfate reactions, (3) gas + sulfate + ternary reactions, and (4) gas + sulfate + NAT reactions, to assess the sensitivity of ClO activation to particle type. NAT particles produced more ClO activation inside the vortex at 46, 31, and 21 hPa than ternary droplets (see Figure 11). From Figures 11 and 12 it is apparent that the sulfate aerosol accounted for a major portion of the chlorine activation at 46, 68, and 100 hPa inside the vortex and for most of the chlorine activation outside the vortex at all of the pressure levels.

Calculations for the gas + sulfate + NAT case illustrated the sensitivity of chlorine activation to reaction probability, reaction pathway, temperature, and surface area specifications. Vortex averaged activation of ClO decreased by 0.3 ppbv at 31 and 46 hPa (see Figure 9) when reaction pathways (8), (9), and (10) and the *Hanson* [1998] reaction probabilities were utilized. The sensitivity of ClO activation to temperature uncertainties increased as pressure decreased (see Figure 10). A uniform temperature reduction of 2 K enhanced peak vortex averaged ClO

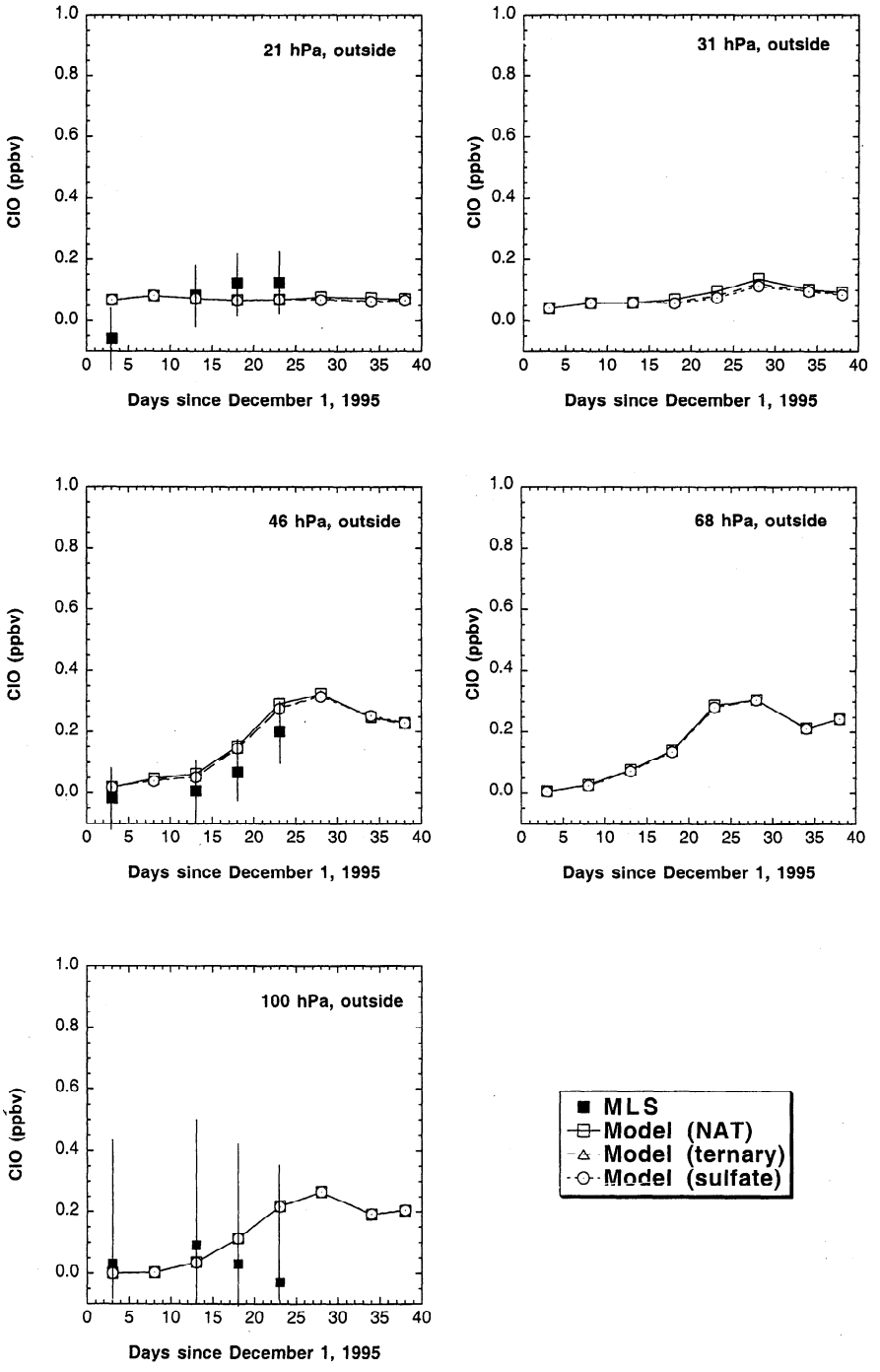

Figure 12. The averaging of the data includes latitudes between 40° North and the edge of the polar vortex. The "NAT," "ternary," and "sulfate" values are for the chemistry as in Figure 11.

activation by 0.4 ppbv at 21 hPa. ClO activation decreased by ~ 0.1 ppbv at 31, 46, and 68 hPa when the sulfate area density was decreased by 30% (see Figure 10).

Time trends of 5-day averages of model and MLS version 4 ClO over extended regions inside and outside the vortex at 21 and 46 hPa agreed within the experimental error (near 0.1 ppbv) for the majority of the averages presented in Figures 11 and 12. The comparisons of model and observations at 100 hPa were problematic because of the large error bars of the MLS ClO data. An overall impression given by the calculations is that the gas phase and heterogeneous chemistry utilized in this model can adequately produce ClO in the Arctic polar regions since both the magnitude and the rate at which ClO is generated by the model agree fairly well with the MLS observations.

Acknowledgments. This work was funded by NASA UARS Science Investigations Program grant S-10103-X. The work of XueXi Tie and Guy Brasseur is supported in part by the DOE Atmospheric Chemistry Program under grant DE-AI05-98ER62579. Work at the Jet Propulsion Laboratory, California Institute of Technology, was done under contract

with NASA. We wish to thank Azadeh Tabazadeh for forwarding to us a copy of the APCM code. The advice given by David Hanson on heterogeneous reaction probabilities is greatly appreciated. The National Center for Atmospheric Research (NCAR) is sponsored by the National Science Foundation.

References

Barath, F. T., et al., The Upper Atmosphere Research Satellite Microwave Limb Sounder Instrument, *J. Geophys. Res.*, *98*, 10,751-10,762,1993.

Brasseur, G., M. H. Hitchman, S. Walters, M. Dymek, E. Falise, and M. Pirre, An interactive chemical dynamical radiative two-dimensional model of the middle atmosphere, *J. Geophys. Res.*, *95*, 5639-5655, 1990.

Brasseur, G. P., X. Tie, P. J. Rasch, and F. Lefevre, A three-dimensional simulation of the Antarctic ozone hole: Impact of anthropogenic chlorine on the lower stratosphere and upper troposphere, *J. Geophys. Res.*, *102*, 8909-8930, 1997.

Carslaw, K. S., B. Luo, and T. Peter, An analytic expression for the composition of aqueous HNO_3-H_2SO_4 stratospheric aerosols including gas phase removal of HNO_3, *Geophys. Res. Lett.*, *22*, 1877-1880, 1995.

Carslaw, K. S., M. Wirth, A. Tsias, B. P. Luo, A. Dornback, M. Leuybecher, H. Volkert, W. Ranger, J. T. Bacmeister, E. Reimer, and T. Peter, Increased stratospheric ozone depletion due to mountain-induced atmospheric waves, *Nature*, *391*, 675-678, 1998.

Chartrand, D. J., and J. C. McConnell, Evidence for HBR production due to minor channel branching at midlatitudes, *Geophys. Res. Lett.*, *25*, 55-58, 1998.

Chipperfield, M. P., D. Cariolle, P. Simon, R. Ramararoson, and D. J. Lary, A three-dimensional modeling study of trace species in the Arctic lower stratosphere during winter 1989-1990, *J. Geophys. Res.*, *98*, 7199-7218, 1993.

Chipperfield, M. P., M. L. Santee, L. Froidevaux, G. L. Manney, W. G. Read, J. W. Waters, A. E. Roche, and J. M. Russell, Analysis of UARS data in the southern polar vortex in September 1992 using a chemical transport model, *J. Geophys. Res.*, *101*, 18861-18881, 1996.

DeMore, W. B., et al., Chemical kinetics and photochemical data for use in stratospheric modeling: Evaluation number 12, *JPL Publ. 97-4*, Jet Propul. Lab., Pasadena, Calif., 1997.

Deniel, C., R. M. Bevilacqua, J. P. Pommereau, and F. Lefevre, Arctic chemical ozone depletion during the 1994-1995 winter deduced from POAM II satellite observations and the REPROBUS three-dimensional model, *J. Geophys. Res.*, *103*, 19231-19244, 1998.

Donaldson, D. J., A. R. Ravishankara, and D. R. Hanson, Detailed study of HOCl + HCl -> Cl_2 + H_2O in sulfuric acid, *J. Phys. Chem.*, *101*, 4717-4725, 1997.

Douglass, A. R., R. B. Rood, J. Waters, L. Froidevaux, W. Read, L. Elson, M. Geller, Y. Chi, M. Cernglia, and S. Steenrod, A 3-D simulation of the early winter distribution of reactive chlorine in the north polar vortex, *Geophys. Res. Lett.*, *20*, 1271-1274, 1993.

Geller, M. A., V. Yudin, A. R. Douglass, J. W. Waters, L. S. Elson, A. E. Roche, and J. M. Russell III, UARS PSC, ClONO2, HCl, and ClO measurements in early winter: Additional verification of the paradigm for chlorine activation, *Geophys. Res. Lett.*, *22*, 2937-2940, 1995.

Glaccum, W., et al., The Polar Ozone and Aerosol Measurement Instrument, *J. Geophys. Res.*, *101*, 14,479-14,487, 1996.

Hanson, D. R., Reaction of $ClONO_2$ with H_2O and HCl in sulfuric acid and HNO_3/H_2SO_4/H_2O mixtures, *J. Phys. Chem.*, *102*, 4794-4807, 1998.

Hanson, D. R., and A. R. Ravishankara, Reactive Uptake of $ClONO_2$ onto sulfuric acid due to reaction with HCl and H_2O, *J. Phys. Chem.*, *98*, 5728-5735, 1994.

Hanson, D. R., A. R. Ravishankara, and S. Solomon, Heterogeneous reactions in sulfuric acid aerosols: A framework for model calculations, *J. Geophys. Res.*, *99*, 3615-1629, 1994.

Kegley-Owen, C. S., Laboratory studies of Cl and ClO radical reactions of atmospheric importance, Ph.D thesis, Dep. of Chem. and Biochem., Univ. of Colo., Boulder, 1998.

Kegley-Owen, C. S., M. K. Gilles, J. B. Burkholder, and A. R., Ravishankara, Rate coefficient measurements for the reaction OH + ClO -> Products, *J. Phys. Chem. A*, *103*, 5040-5048, 1999.

Lipson, J. B., T. W. Beiderhase, L. T. Molina, M. J. Molina, and M. Olzmann, Production of HCl in the OH + ClO reaction: Laboratory measurements and statistical rate theory calculations, *J. Phys. Chem. A*, *103*, 6540-6551, 1999.

Lumpe, J. D., et al., POAM II retrieval algorithm and error analysis, *J. Geophys. Res.*, *102*, 23,593-23,614, 1997.

Manney, G. L., et al., Chemical depletion of ozone in the Arctic lower stratosphere during winter 1992-1993, *Science*, *370*, 429-434, 1994.

Manney, G. L., R. Swinbank, S. T. Massie, M. E. Gelman, A. J. Miller, R. Nagatani, A. O'Neil, and R. W. Zurek, Comparison of UKMO and NMC stratospheric analyses during northern and southern winter, *J. Geophys. Res.*, *101*,10,311-10,334, 1996.

Massie, S. T., et al., Simultaneous observations of polar stratospheric clouds and HNO_3 over Scandinavia in January 1992, *Geophys. Res. Lett.*, *24*, 595-598, 1997.

Massie, S. T., D. Baumgardner, and J. E. Dye, Estimation of polar stratospheric cloud volume and area densities from UARS, stratospheric aerosol measurement II, and polar ozone and aerosol measurement II extinction data, *J. Geophys. Res.*, *103*, 5773-5783, 1998.

McElroy, M. B., and R. J. Salawitch, Changing composition of the global stratosphere, *Science*, *243*, 763-770, 1989.

Michelsen, H. A., et al., Stratospheric chlorine partitioning: Constraints from shuutle-borne measurements of [HCl], [$ClNO_3$], and [ClO], *Geophys. Res. Lett.*, *23*, 2361-2364, 1996.

Nash, E. R., P. A. Newman, J. E. Rosenfield, and M. R. Schoeberl, An objective determination of the polar vortex using Ertel's potential vorticity, *J. Geophys. Res.*, *101*, 9471-9478, 1996.

Park, J. H., et al., Validation of Halogen Occultation Experiment CH_4 measurements from the UARS, *J. Geophys. Res.*, *101*, 10,183-10,203, 1996.

Portmann, R. W., S. Solomon, R. R. Garcia, L. W. Thomason, L. R. Poole, and M. P. McCormick, Role of aerosol variations in anthropogenic ozone depletion in the polar regions, *J. Geophys. Res.*, *101*, 22,991-23,006, 1996.

Pullen, S., and R. L. Jones, Accuracy of temperatures from UKMO analyses of 1994/1995 in the arctic winter stratosphere, *Geophys. Res. Lett.*, *24*, 845-848, 1997.

Randall, C. E., D. W. Rusch, J. J. Olivero, R. M. Bevilacqua, L. R. Poole, J. D. Lumpe, M. D. Fromm, K. W. Hoppel, J. S. Hornstein, and E. P. Shettle, An overview of POAM II aerosol measurements at 1.06 μm, *Geophys. Res. Lett.*, *23*, 3195-3198, 1996.

Ravishankara, A. R., and D. R. Hanson, Differences in the reactivity of Type I polar stratospheric clouds depending on their phase, *J. Geophys. Res.*, *101*, 3885-3890, 1996.

Russell, J. M., III, L. L. Gordley, J. H. Park, S. R. Drayson, W. D. Hesketh, R. J. Cicerone, A. F. Tuck, J. E. Frederick, J. E. Harries, and P. J. Crutzen, The Halogen Occultation Experiment, *J. Geophys. Res.*, *98*, 10,777-10,797, 1993.

Russell, J. M., III, et al., Validation of hydrogen chloride measurements made by the Halogen Occultation Experiment from the UARS platform, *J. Geophys. Res.*, *101*, 10,151-10,162, 1996.

Salawitch, R. J., et al., Chemical loss of ozone in the Arctic Polar Vortex in the winter of 1991-1992, *Science*, *261*, 1146-1149, 1993.

Santee, M. L., W. G. Read, J. W. Waters, L. Froidevaux, G. L. Manney, D. A. Flower, R. F. Jarnot, R. S. Harwood, and G. E. Peckham, Interhemispheric differences in polar stratospheric HNO_3, H_2O, ClO, and O_3, *Science*, *267*, 849-852, 1996.

Santee, M. L., A. Tabazadeh, G. L. Manney, R. J. Salawitch, L. Froidevaux, W. G. Read, and J. W. Waters, UARS Microwave Limb Sounder HNO_3 observations: Implications for Antarctic polar stratospheric clouds, *J. Geophys. Res.*, *103*, 13,285-13,313, 1998.

Santee, M. L., G. L. Manney, L. Froidevaux, W. G. Read, and J. W. Waters, Six years of UARS Microwave Limb Sounder HNO_3 observations: Seasonal, interhemispheric, and interannual variations in the lower stratosphere, *J. Geophys. Res.*, *104*, 8225-8246, 1999.

Schoeberl, M. R., L. R. Lait, P. A. Newman, and J. E. Rosenfield, The structure of the polar vortex, *J. Geophys. Res.*, *97*, 7859-7882, 1992.

Schoeberl, M. R., R. S. Stolarski, A. R. Douglass, P. A. Newman, L. R. Lait, J. W. Waters, L. Froidevaux, and W. G. Read, MLS ClO observations and Arctic polar vortex temperatures, *Geophys. Res. Lett.*, *20*, 2861-2864, 1993.

Sessler, J., P. Good, A. R. MacKenzie, and J. A. Pyle, What role do type I polar stratospheric cloud and aerosol parameterizations play in modelled lower stratospheric chlorine activation and ozone loss?, *J. Geophys. Res.*, *101*, 28,817-28,835, 1996.

Smolarkiewicz, P., and P. J. Rasch, Monotone advection on the sphere:

An Eulerian versus semi-Lagrangian approach, *J. Atmos. Sci.*, *48*, 793-810, 1991.

Swinbank, R., and A. O'Neill, A stratosphere-troposphere data assimilation system, *Month. Wea. Rev.*, *122*, 686-702, 1994.

Tabazadeh, A., R. P. Turco, and M. Z. Jacobson, A model for studying the composition and chemical effects of stratospheric aerosols, *J. Geophys. Res.*, *99*, 12,897-12,914, 1994.

Thomason, L. W., L. R. Poole, and T. Deshler, A global climatology of stratospheric surface area density deduced from stratospheric aerosol and gas experiment II measurements: 1984-1994, *J. Geophys. Res.*, *102*, 8967-8976, 1997.

Waters, J. W., et al., Validation of UARS Microwave Limb Sounder ClO Measurements, *J. Geophys. Res.*, *101*, 10,091-10,127, 1996.

Waugh, D. W., and W. J. Randel, Climatology of Arctic and Antarctic polar vortices using elliptical diagnostics, *J. Atmos. Sci.*, in press, 1999.

World Meterological Organization, *Scientific Assessment of Ozone Depletion: 1991*, Geneva, Switzerland, 1991.

World Meterological Organization, *Scientific Assessment of Ozone Depletion: 1994*, Geneva, Switzerland, 1995.

Worsnop, D. R., L. E. Fox, M. S. Zahniser, and S. C. Wofsy, Vapor pressures of solid hydrates of nitric acid, Implications for polar stratospheric clouds, *Science*, *259*, 71-74, 1993.

Yudin, V. A., M. A. Geller, B. V. Khattatov, A. R. Douglass, M. C. Cerniglia, J. W. Waters, L. S. Elson, A. E. Roche, and J. M. Russell III, A UARS study of lower stratospheric polar processing in the early stages of northern southern winters, *J. Geophys. Res.*, *102*, 19,137-19,148, 1997.

R. M. Bevilacqua and M. D. Fromm, Naval Research Laboratory, 4555 Overlook Ave S.W., Washington, DC 20375.

G. P. Brasseur, S. T. Massie, and X. Tie, National Center for Atmospheric Research, P. O. Box 3000, Boulder, CO 80307. (massie@ncar.ucar.edu)

M. L. Santee, Jet Propulsion Laboratory, California Institute of Technology, 4800 Oak Grove Drive, Pasadena, CA 91109.

(Received March 30, 1999; revised October 1, 1999;
accepted October 7, 1999.)